Theoretical and Experimental Studies of the Response of Rubble-mound Breakwater due to Earthquakes

by

Hsiang Wang, Shi-Shuenn Chen and C. Y. Yang

Ocean Engineering Report No. 10

August 1976

Department of Civil Engineering
University of Delaware
Newark, Delaware

Sponsored by the U. S. Nuclear Regulatory Commission, ERDA, under Contract Numbers E (11-1)-207 and AT (49-24)-310.

ACKNOWLEDGMENTS

The authors are grateful to Dr. Robert Dean for his comments on the theoretical work, to Dr. R. B. Pipes for his assistance in the calibration of the accelerometer, to Mr. James Coverdale, Mr. Roland Essex and Mr. John Mark for their assistance throughout the experimental work. Thanks are also due to Mr. Craig Lamison whose thesis work prior to this investigation was most helpful in the experimental phase, to Mr. T. C. Ho for his comments in the final phase of the analytic work and to Mrs. Susan Sulpizi and Mrs. Barbara Shelton for typing and other secretarial assistance.

The work is part of the ERDA Breakwater Safety study under Contract Nos. E(11-1)-2707 and AT(49-24)-0310 with the University of Delaware. The financial support is gratefully acknowledged.

TABLE OF CONTENTS

ABSTRACT

Both theoretical and experimental methods are employed to study the hydrodynamic effect of the horizontal earthquake action on rubble-mound breakwaters having either a vertical or inclined front face.

In the theoretical study, an alternative approach for Westergaard's problem, using the concept of frequency and impulse response functions, is presented for the solution of the pressure change on a rigid breakwater with vertical front face. The pressure response of the breakwater to random earthquakes is also investigated in this case. An extension of Von Kármán's approximate theory is made to determine the hydrodynamic pressure on a breakwater with inclined front face.

The experimental study was conducted in the large wave tank of the Civil Engineering Department. An idealized model with vertical faces made of wood was first tested and then followed the scaled model made of gravels and Dolosse (a particular type of surface protection structural elements) with inclined faces. Horizontal accelerations from 0.148 g up to 0.835 g were applied as the dynamic input and the input frequency used was about 2.5 cycles per second.

The experimental results for dynamic pressures are compared to those of the extended Von Kármán's theory and those of Zangar's results including the effect of surface waves. The comparison shows good agreement in the case of vertical faced model but large discrepancies appear in the simulated model with inclined surface.

LIST OF FIGURES

LIST OF PHOTOGRAPHS

LIST OF PHOTOGRAPHS (CONTINUED)

CHAPTER I

INTRODUCTION

The study of the behavior of breakwater structures in earthquakes is complicated by the interaction of the motion of the structure and that of the surrounding water. The movement of the structure and of the other boundaries of the fluid generates pressure waves within the fluid and sometimes significant surface wave effects.

Westergaard [1] was the first one who in 1933 solved the two dimensional case of horizontal vibrations of a rigid dam with vertical upstream face placed at one end of an infinitely long reservoir of uniform depth. He obtained the hydrodynamic pressure on the face of the dam and the water displacement under the assumption that the motion of the dam during earthquakes is simple harmonic and that the displacements are small.

In the same year, 1933, Von Kármán [2] developed an approximate but very simple method to determine the maximum hydrodynamic pressure on the dam due to the same horizontal earthquake motion. Brahtz and Heilbron [3] in 1933 also demonstrated that if the reservoir is of finite length, the pressure increases not more than 0.5% if $\ell/h > 2$,

where ℓ is the length and h is the depth of the reservoir. If the upstream end of the reservoir is assumed to vibrate with the ground, the effect of length is negligible for $\ell/h > 3$. Since $\ell/h > 3$ is satisfied for most dams, the pressure response is thus not sensitive to reservoir length.

In 1949, Werner and Sundquist [4] deduced solutions for some types of hydraulic vessels by taking the compressibility of water into consideration.

In 1952, Zangar [5] determined the hydrodynamic pressures by using an electric analogy and concluded that hydrodynamic pressure on a dam having the upstream face vertical for half or more of the total height is practically the same as when the upstream face is vertical for the full height.

In 1960, Chen-Chzhen Chen [6] further investigated this problem allowing the existence of surface waves in an incompressible fluid.

Most of the previous works ignored the interaction between the deformable dam and the reservoir and little attention was given to the corresponding problem for vertical ground motion. In 1967, Chopra [7] studied the reservoir-dam interaction during earthquakes and also obtained solutions for the hydrodynamic pressure due to vertical ground motion.

In this thesis, taking the compressibility of the water into consideration, a method for determining the hydrodynamic pressure on a rigid breakwater with vertical face in the sea side due to random horizontal earthquakes is developed. Also by assuming that the water is incompressible, a modified Von Karman formulation is derived to determine the hydrodynamic pressure on a rigid breakwater with inclined front face.

With different horizontal accelerations, a series of experiments were carried out to investigate the pressure change on the breakwater. From these experiments the hydrodynamic pressure on the breakwater at free water surface is found not to be zero and as the acceleration is increased the effect of surface wave became more significant and can not be neglected. The deformation of the breakwater was also measured in the experiment.

An electro-hydraulic control system was manipulated in the experiments to actuate a motion representing the horizontal earthquakes and the accelerations used in the experiments varied from 0.148 g to 0.835 g which covered the range of usual earthquake motions.

CHAPTER II

THEORETICAL ANALYSIS

2.1 Westergaard's 1933 Solution [1]

By assuming that water was compressible and invisid and that the fluid displacement was small, Westergaard obtained the following two dimensional steady-state solution for the hydrodynamic pressure on the vertical face of a rigid dam (Figure 1),

$$p = -\frac{8\alpha wh}{\pi^2} \cos\frac{2\pi t}{T} \sum_{1,3,5\ldots}^{n} \frac{1}{n^2 b_n} \sin\frac{n\pi y}{2h} \qquad (1)$$

where p is the dynamic pressure, w is the unit weight of water, h is the depth of water, t is time, y is the vertical distance upward from the base, T is the fundamental period, α is the earthquake coefficient, and b_n is defined by

$$b_n = \sqrt{1 - \frac{16wh^2}{n^2 gK\, T^2}} \qquad (2)$$

in which K is the bulk modulus of water.

2.2 An Alternate Approach to Westergaard's Problem

A. Formulation

Consider a rigid breakwater with a vertical front face, subjected to a horizontal ground acceleration $a_x(t)$, as shown in Figure 1. If we consider the two dimensional case, neglecting the viscosity effect of water, and assume that the displacements in the water body are small, and the motion is irrotationa, then the motion of water is governed by the wave equation [8]:

$$\frac{\partial^2\phi}{\partial x^2} + \frac{\partial^2\phi}{\partial y^2} = \frac{1}{c^2}\frac{\partial^2\phi}{\partial t^2} \tag{3}$$

in which $\phi(x,y,t)$ is the velocity potential, $c = \sqrt{K/\rho}$ is recognized as the velocity of pressure waves in water, K is the bulk modulus of water, and ρ is the density of water.

The hydrodynamic pressure $p(x,y,t)$ is given by:

$$p = -\rho \frac{\partial\phi}{\partial t} \tag{4}$$

If we consider the sea side to be infinitely long and neglect the effect of surface waves, then the boundary conditions are as follows:

$$\phi \text{ is finite as } x \to \infty \tag{5}$$

$$-\frac{\partial^2\phi}{\partial t\partial x}(0,y,t) = a_x(t) \tag{6}$$

$$\frac{\partial\phi}{\partial y}(x,0,t) = 0 \tag{7}$$

$$\frac{\partial\phi}{\partial t}(x,h,t) = 0 \tag{8}$$

and if the reservoir is at rest when earthquake begins, then the initial conditions are:

$$\phi(x,y,0) = 0 \tag{9}$$

$$\frac{\partial \phi}{\partial t}(x,y,0) = 0 \tag{10}$$

B. Solution

By making use of the complex frequency response $H(x,y,\omega)$, Equation (3) can be solved for a steady state acceleration. Let $a_x(t) = e^{i\omega t}$ and the steady state solution be

$$\phi(x,y,t) = H(x,y,\omega)\, e^{i\omega t} \tag{11}$$

and if $a_x(t)$ is the real part of $e^{i\omega t}$, then the response is the real part of $H(x,y,\omega)\, e^{i\omega t}$. Substituting Equation (11) into (3), gives:

$$\frac{\partial^2 H}{\partial x^2} + \frac{\partial^2 H}{\partial y^2} = -\frac{\omega^2}{c^2} H \tag{12}$$

Since the derivatives are not taken with respect to ω, we can solve H as a function of x and y with ω as a parameter such that $H(x,y,\omega)$ satisfies the boundary conditions. The above boundary conditions are then transformed to be:

$$H \text{ is finite as } x \to \infty \tag{13}$$

$$\frac{\partial H}{\partial x}(0.y) = \frac{i}{\omega} \tag{14}$$

$$\frac{\partial H}{\partial y}(x,0) = 0 \tag{15}$$

$$H(x,h) = 0 \tag{16}$$

Substituting $H(x,y) = X(x)Y(y)$ into Equation (12), gives:

$$X''Y + Y''X = -\frac{\omega^2}{c^2} X Y$$

Dividing both sides of the above equation by X Y gives:

$$\frac{X''}{X} + \frac{Y''}{Y} = -\frac{\omega^2}{c^2}$$

or

$$\frac{X''}{X} + \frac{\omega^2}{c^2} = -\frac{Y''}{Y} = \lambda_n^2 \tag{17}$$

where λ_n is a constant.

From Equation (17), one can get the following two equations:

$$X'' - (\lambda_n^2 - \frac{\omega^2}{c^2}) X = 0 \tag{18}$$

$$Y'' + \lambda_n^2 Y = 0 \tag{19}$$

From Equation (18) yields

$$X(x) = c_1 e^{\sqrt{\lambda_n^2 - \frac{\omega^2}{c^2}}\, x} + c_2 e^{-\sqrt{\lambda_n^2 - \frac{\omega^2}{c^2}}\, x}$$

From Equation (19) yields

$$Y(y) = c_3 \sin \lambda_n y + c_4 \cos \lambda_n y$$

Hence,

$$H(x,y) = \left(c_1 e^{\sqrt{\lambda_n^2 - \frac{\omega^2}{c^2}}\, x} + c_2 e^{-\sqrt{\lambda_n^2 - \frac{\omega^2}{c^2}}\, x}\right)$$

$$(c_3 \sin \lambda_n y + c_4 \cos \lambda_n y) \qquad (20)$$

Making use of the boundary conditions on $H(x,y,\omega)$, we obtain:

from (13), $c_1 = 0$

from (15), $c_3 = 0$

from (16), $\lambda_n = \frac{2n-1}{2h}\pi$

Therefore,

$$H(x,y,\omega) = c_2 e^{-\sqrt{\lambda_n^2 - \frac{\omega^2}{c^2}}\, x} (c_4 \cos \lambda_n y)$$

or

$$H(x,y,\omega) = c_n e^{-\sqrt{\lambda_n^2 - \frac{\omega^2}{c^2}}\, x} \cos \lambda_n y$$

Since Equation (12) is linear, it follows that any linear combination of such solutions will also satisfy (12). Accordingly, let

$$H(x,y,\omega) = \sum_{n=1}^{\infty} c_n \, e^{-\sqrt{\lambda_n - \frac{\omega^2}{c^2}}\, x} \cos \lambda_n y \qquad (21)$$

From boundary condition (14),

$$\sum_{n=1}^{\infty} c_n \left(-\sqrt{\lambda_n^2 - \frac{\omega^2}{c^2}}\right) \cos \lambda_n y = \frac{i}{\omega}$$

Since the functions on the left-hand side of the above equation form a complete orthogonal set, it follows:

$$\int_0^h \sum_{n=1}^{\infty} c_n \sqrt{\lambda_n^2 - \frac{\omega^2}{c^2}} \cos \lambda_n y \cos \lambda_m y \, dy = \frac{i}{\omega} \int_0^h \cos \lambda_m y \, dy$$

and hence

$$c_n = \frac{4}{i\omega\pi} \frac{(-1)^{n-1}}{\sqrt{\lambda_n^2 - \frac{\omega^2}{c^2}}\,(2n-1)} \qquad (22)$$

Substituting (22) into (21), follows

$$H(x,y,\omega) = \frac{4}{i\omega\pi} \sum_{n=1}^{\infty} \frac{(-1)^{n-1}}{(2n-1)\sqrt{\lambda_n^2 - \frac{\omega^2}{c^2}}} \exp\{-\sqrt{\lambda_n^2 - \frac{\omega^2}{c^2}}\, x\} \cos \lambda_n y \qquad (23)$$

From Equations (4), (11), and (23), the pressure can be obtained.

$$p(x,y,t) = \{\frac{4\rho}{\pi} \sum_{n=1}^{\infty} \frac{(-1)^{n-1}}{(2n-1)\sqrt{\lambda_n^2 - \frac{\omega^2}{c^2}}} \exp[-\sqrt{\lambda_n^2 - \frac{\omega^2}{c^2}}\, x] \cos \lambda_n y\}\, e^{i\omega t} \tag{24}$$

On the other hand, by definition,

$$p(x,y,t) = H_p(x,y,\omega)\, e^{i\omega t}, \text{ then}$$

$$H_p(x,y,\omega) = \frac{4\rho}{\pi} \sum_{n=1}^{\infty} \frac{(-1)^{n-1}}{(2n-1)\sqrt{\lambda_n^2 - \frac{\omega^2}{c^2}}} \exp\{-\sqrt{\lambda_n^2 - \frac{\omega^2}{c^2}}\, x\} \cos \lambda_n y \tag{25}$$

If now $a_x = -\alpha g \cos \omega t$, in which α is a constant, then the pressure on the front surface of the breakwater is

$$p(0,y,t) = -\frac{4\alpha\rho g}{\pi} \cos \omega t \sum_{n=1}^{\infty} \frac{(-1)^{n-1}}{(2n-1)\sqrt{\lambda_n^2 - \frac{\omega^2}{c^2}}} \cos \lambda_n y \tag{26}$$

which is exactly the same as the corresponding result of Westergaard.

2.3 Approximate Theory for Breakwater--Extension of Von Kármán's Theory [9]

A. Formulation

Consider a unit slice of a breakwater with an inclined front face, with the height, h, and infinite length, as shown in Figure 2.

Assume that the breakwater is at rest when $t = 0$, and that uniform horizontal acceleration, a_x, is acting during the time interval, Δt, and that a portion of the incompressible fluid with a width, b, has a constant mean acceleration a_{xf}, while the remainder of the fluid is not affected in the motion process.

1. Continuity of Fluid Flow: Assume that the vertical acceleration of the fluid is variable with the height and has the mean value (horizontally averaged), a_y, between B and C. Then the horizontal displacement of the breakwater during the time, Δt, is $a_x \Delta t^2/2$ and the vertical displacement of the fluid through the section BC is $a_y \Delta t^2/2$. The condition of continuity requires that

$$y\left(a_x \frac{\Delta t^2}{2}\right) = b\left(a_y \frac{\Delta t^2}{2}\right)$$

or

$$y\, a_x = b\, a_y \tag{27}$$

2. Equation of motion:

x-direction: Let the pressure at an arbitrary height, y, be p and the density of the fluid be ρ, then from Figure 3, the equilibrium of horizontal dynamic forces requires that

$$p\, ds \sin\theta = (\rho\, b\, dy)\, a_{xf}$$

or

$$p = \rho\, b\, a_{xf} \tag{28}$$

y-direction: In Figure 3, the resultant force on the bottom surface of the element equals pb, that on the top surface is equal to $pb + \frac{d}{dy}(pb)dy$, and the component of the force acting on ds along the y-direction is p ds cos θ, hence

$$p\ ds\ \cos\theta - \frac{d}{dy}(pb)\ dy = (\rho\ b\ dy)\ a_y$$

or

$$p\ \cot\theta - p\ \frac{db}{dy} - b\ \frac{dp}{dy} = \rho\ b\ a_y \qquad (29)$$

3. Boundary Conditions:

on water surface:

$$p = 0 \quad \text{at} \quad y = h$$

on the inclined front face: Since the slip of the fluid on the surface of the breakwater should be taken into account and for the special case of a breakwater with a vertical front face, the constant mean horizontal acceleration of the fluid, a_{xf}, must be equal to the horizontal acceleration of the breakwater, a_x, as shown in Figure 4, it is reasonable to assume that

$$a_{xf} = a_x \sin^2\theta \qquad (30)$$

B. Solution

It is observe that Equations (27) through (30) constitute a system of four equations with four unknowns p, b, a_{xf} and a_y which can be solved as follows: Substituting Equations(27), (28) and (30) into (29), gives a single equation for the width of the apparent mass, b,

$$\frac{b}{2} \sin 2\theta - 2b \sin^2\theta \frac{db}{dy} = y \qquad (31)$$

To solve for b, let the new variable v be defined by $y = vb$, then $dy = vdb + bdv$. Substituting y and dy into Equation (31), dividing all terms by b^2 and separating terms with db from those with dv, gives

$$(v^2 - \frac{v}{2} \sin 2\theta + 2 \sin^2 \theta) \frac{db}{b} + (v - \frac{1}{2} \sin 2\theta)\, dv = 0$$

or

$$\frac{dv}{\phi(v)} + \frac{db}{b} = 0 \qquad (32)$$

where

$$\phi(v) = v + \frac{4 \sin^2\theta}{2v - \sin 2\theta}$$

The exact solution of Equation (32) with the integration constant, k, is [10]:

$$\ell n \frac{k}{b} = \int \frac{dv}{\phi(v)}$$

or

$$\ell n \frac{k}{b} = \frac{1}{2} \ell n|2 v^2 - v \sin 2\theta + 4 \sin^2\theta|$$

$$- \frac{\cos\theta}{\sqrt{8 - \cos^2\theta}} \tan^{-1} \frac{4v - \sin 2\theta}{2\sin\theta\sqrt{8 - \cos^2\theta}} \qquad (33)$$

Since the boundary condition requires $p = 0$, hence $b = 0$, at $y = h$, the intergration constant k determined by Equation (33) is

$$k^2 = 2h^2 \exp\{-\frac{\pi \cos\theta}{\sqrt{8 - \cos^2\theta}}\} \tag{34}$$

Equations (33) and (34) constitute the required exact solution for b as a function of y.

C. Comparison With Westergaard's Solution

For $\theta = 90°$, from Equations (34) and (33), it follows

$$k^2 = 2h^2$$
$$b = 0.707\sqrt{h^2 - y^2} \tag{35}$$

then, from (28), (30) and (35), the dynamic pressure on the bottom of the breakwater where $y = 0$ is found:

$$p = 0.707\ \alpha\ wh \tag{36}$$

From Equation (1) and the fact that for $T > 1$ sec, all the b_n's are very close to 1, the maximum pressure at the bottom of the breakwater is

$$p_{max} \approx \frac{8\ \alpha\ wh}{\pi^2} \sum_{1,3,5\ldots}^{n} \frac{(-1)^{\frac{n-1}{2}}}{n^2},$$

or

$$p_{max} \approx 0.743\ \alpha\ wh \tag{37}$$

The difference between the pressures calculated from (36) and (37) is about 4 or 5 percent.

2.4 Solution for Random Earthquakes

Assume that the whole system is linear, then the complex frequency response $H(x,y,\omega)$ is the Fourier transform of the unit impulse response $h(x,y,t)$[11]. The Fourier integral representation of the unit impulse pressure response is then [12]:

$$h_p(x,y,t) = \frac{1}{2\pi} \int_{-\infty}^{\infty} H_p(x,y,\omega)\, e^{i\omega t}\, d\omega$$

$$= \begin{cases} 0 & , \quad t < \frac{x}{c} \\ \frac{4\rho c}{\pi} \sum_{n=1}^{\infty} \frac{(-1)^{n-1}}{2n-1} \cos \lambda_n y \cdot J_o(\lambda_n \sqrt{(ct)^2 - x^2}) & , \quad t > \frac{x}{c} \end{cases} \tag{38}$$

where J_o is the first kind Bessel function of zero order.

The unit impulse response for the hydrodynamic pressure on the breakwater is then:

$$h_p(0,y,t) = \frac{4\rho c}{\pi} \sum_{n=1}^{\infty} \frac{(-1)^{n-1}}{2n-1} \cos \lambda_n y \cdot J_o(\lambda_n ct) \quad , \quad t > 0 \tag{39}$$

The hydrodynamic pressure on the breakwater due to the horizontal earthquake $a_x(t)$ can be obtained from Equation (39) by the following convolution integral:

$$p(0,y,t) = \int_o^t a_x(\tau)\, h_p\,(0,y,t-\tau)\, d\tau \tag{40}$$

Substituting (39) into (40), gives

$$p(0,y,t) = \frac{4\rho c}{\pi} \sum_{n=1}^{\infty} \frac{(-1)^{n-1}}{2n-1} \cos \lambda_n y \int_o^t a_x(\tau)\, J_o\{\lambda_n c(t-\tau)\}d\tau \quad (41)$$

If, furthermore, assume that $a_x(t)$ is Gaussian, then it can be shown that the response $p(0,y,t)$ is also Gaussian [11]. For a Guassian process, only the mean and the covariance are required to characterize the complete process [11].

If the ensemble average $< a_x(\tau) > = 0$, then

$$< p(0,y,t) > = \frac{4\rho c}{\pi} \sum_{n=1}^{\infty} \frac{(-1)^{n-1}}{2n-1} \cos \lambda_n y \int_0^t <a_x(\tau)>\ J_o\{\lambda_n c(t-\tau)\}d\tau = 0$$

and the variance

$$\sigma_p^{\,2}(0,y,t) = <[p(0,y,t) - < p(0,y,t)>]^2 > = < p^2(0,y,t)> \quad (42)$$

Substituting Equations (40) and (42), gives

$$\sigma_p^{\,2}(0,y,t) = \int_0^t \int_0^t < a_x(\tau_1)\, a_x(\tau_2) > h_p(0,y,t-\tau_1)\, h_p(0,y,t-\tau_2)d\tau_1\, d\tau_2$$

$$= \int_0^t \int_0^t R_{a_x}(\tau_1 - \tau_2)\, h_p(0,y,t-\tau_1)\, h_p(0,y,t-\tau_2)\, d\tau_1\, d\tau_2 \quad (43)$$

where R_{a_x} is the autocorrelation function of the input acceleration.

Since

$$R_{a_x}(\tau_1 - \tau_2) = \int_{-\infty}^{\infty} S_{a_x}(\omega)\, e^{i\omega(\tau_1 - \tau_2)}\, d\omega \tag{44}$$

where S_{a_x} is the power spectral density function of a_x.

Substituting (39) and (44) into (43), it follows

$$\sigma_p^2(0,y,t) = \frac{16\,\rho^2 c^2}{\pi^2} \sum_{n=1} \frac{(-1)^{n-1}}{2n-1} \cos \lambda_n y \sum_{m=1}^{\infty} \frac{(-1)^{m-1}}{2m-1} \cos \lambda_m y \int_0^t \int_0^t \int_{-\infty}^{\infty}$$

$$S_{a_x}(\omega)\, e^{i\omega(\tau_1 - \tau_2)} J_o\{\lambda_n c(t-\tau_1)\} J_o\{\lambda_n c(t-\tau_2)\}\, d\omega d\tau_1\, d\tau_2 \tag{45}$$

Since the mean of $p(0,y,t)$ is zero, the covariance of $p(0,y,t)$ is equal to its autocorrelation function $R_p(\tau)$ and $R_p(\tau)$ can be determined as follows [13]:

$$R_p(\tau) = \langle p(0,y,t)\, p(0,y,t+\tau) \rangle$$

$$= \left\langle \int_{-\infty}^{\infty} a_x(\theta_1)\, h_p(0,y,\, t-\theta_1) d\theta_1 \int_{-\infty}^{\infty} a_1(\theta_2)\, h_p(0,y,\, t+\tau-\theta_2) d\theta_2 \right\rangle$$

$$= \int_{-\infty}^{\infty} \int_{-\infty}^{\infty} R_{a_x}(\tau - u_2 + u_1) h_p(0,y,u_1) h_p(0,y,u_2)\, du_1\, du_2 \tag{46}$$

where $u_1 = t - \theta_1$

$u_2 = t + \tau - \theta_2$

Substituting (39) into (46) gives

$$R_p(\tau) = \frac{16\,\rho^2 c^2}{\pi^2} \sum_{n=1}^{\infty} \frac{(-1)^{n-1}}{2n-1} \cos \lambda_n y \sum_{m=1}^{\infty} \frac{(-1)^{m-1}}{2m-1} \cos \lambda_m y \cdot$$

$$\cdot \int_{-\infty}^{\infty} \int_{-\infty}^{\infty} R_{a_x}(\tau - u_2 + u_1)\, J_o(\lambda_n c\, u_1)\, J_o(\lambda_m c\, u_2)\, du_1\, du_2 \qquad (47)$$

Then, making use of Equations (45) and (47), the process $p(0,y,t)$ can be completely characterized.

2.5 The Unsolved Problem

In the extension of Westergaard's solution, what we have considered is a breakwater with vertical front face (Figure 1). If it is changed to be an inclined surface making an angle θ with the horizontal base, then the boundary condition (6) becomes:

$$-\frac{\partial^2 \phi}{\partial t \partial x} = a_x(t) \quad \text{on } y = -x \tan \theta$$

$$\text{where } 0 \leq y \leq h$$

The new boundary condition makes this problem difficult to solve and so far, to our knowledge, there is no analytical solution available.

CHAPTER III

EXPERIMENTS

Craig Lamison made an experimental study on the response of the rubble-mound breakwater due to earthquake. He concentrated his studies on the deformed profile of the breakwater. Here the emphasis is on the dynamic pressure changes on the breakwater due to earthquakes. The basic experimental set-up is similar to that of Laminson's [14].

3.1 Model Construction and Earthquake Selection

The experiments were divided into two groups. In the first group, a model breakwater with a vertical front face was tested to measure the pressure change on the front face at different elevations. In the second group, a model with a 30° inclined front face was tested.

The mode with the inclined faces was made in three layers, the outer armor layer, the armor sublayer, and the inner core. The dimension of the model is shown in Figure 5. A total of 450 pieces of "Dolosse" (a special construction unit as shown in Photograph 9) were used for the armor layer and the larger stone for the armor sublayer was composed as follows:

TABLE 1

Armor Sublayer Stone Scaling

Average Weight oz./stone	Percent %	Retain on Seive Size
3.8	22	1.50
1.5	59	1.05
0.65	17	0.625
0.17	2	<0.625

The inner core stone was composed as follows:

TABLE 2

Inner Core Stone Scaling

Average Weight oz./stone	Percent %	Retain on Seive Size
0.066	27	0.371
0.026	49	0.25
0.010	18	0.187
0.0042	6	<0.187

In the first group of the tests, two vertical wooden walls were fixed on both sides of the model, on which four holes were drilled so that the pressure transducers can be mounted there.

The frequency of the simulated earthquake ground motion in the experiments was selected to be 2.5 cycles per second and the amplitudes were varied such that the simulated horizontal accelerations varied from 0.148 g to 0.835 g.

3.2 Experimental Setup and Procedures

The model breakwater was tested in a wave tank measured 5 feet deep by 7 feet - 8 inches wide and about 100 feet long as shown in Photograph 2.

The loading actuator, as shown in Photograph 1, is a 20 kip Gilmore hydraulic model with a Moog 72-102, 40 gallon per minute Servo-valve and is attached to the shake table [14] which is designed to support and impart motion to the model breakwater and is situated in the center of the wave tank.

The actuator is controlled by a Gilmore, Model 431 B Servo-Controller and a Model 112 Function Generator (or Wavetek)[14] as shown in Photograph 5. Single pulse and multiple cycle commands can be triggered manually or automatically. The Servo-Controller at all times monitors the response of the actuator.

A Statham, Model A5, accelerometer is mounted on the shake table to measure the acceleration of the earthquake motion actuated, as shown in Photograph 3. The most sensitive direction of the accelerometer is put in line with that of the simulated earthquake motion.

A Statham, Model P131, pressure transducer and a Viatran, Model 103, pressure transducer are fixed on the model breakwater to measure the hydrodynamic pressure on the surface of the breakwater, as shown in Photograph 4.

A Vishay, Model BAM-1, Bridge Amplifier Meter was used to monitor signals from the accelerometer on the oscilloscope and two Viatram, Model 601, amplifiers were used for the two pressure transducers, as shown in Photograph 5. A Tekelec, Model TA357, volt meter was also used to ensure the excitation of the accelerometer to be kept exactly at 11 volts.

The pressure responses and the earthquake pulse command were monitored by a Type 564, Tektronix oscilloscope and recorded by a Tektronix, Type C-12, oscilloscope camera with Polaroid Type 47 film.

A nine volt battery and switch triggered the oscilloscope trace and the Function Generator through a General Radio Type 1531-P2 photographic flash delay [14]. The flash delay can retard the Wavetek command pulse between 0.001 and 0.8 seconds and was set as needed to ensure that the oscilloscope trace had time to come on the Cathode-ray Tube before the command was generated.

For both models, breakwater with vertical faces and inclined faces, as shown in Photograph 7and 8, respectively, pressure change on the surface of the breakwater at four different elevations were

measured. However, since only two pressure transducers were available for the experiments, pressure changes at two elevations on the surface of the breakwater were measured each time. A new model was reconstructed to ensure an identical profile for the remaining two pressure measurements. The water level in all tests was kept to be 18.5 inches measured from the bottom of the model breakwater.

The experimental progress and procedures are summarized as follows:

(1) Calibrate the accelerometer and the pressure transducers [Appendix 1].

(2) Build the model of the breakwater.

(3) Mount the accelerometer on the shake table and the pressure transducers on the breakwater.

(4) Fill water to the required level.

(5) Connect the accelerometer and the pressure transducers to the oscilloscope.

(6) Calibrate the oscilloscope [Appendix 2].

(7) Turn on the power and start the actuator.

(8) Set frequency and amplitude on the Servo-controller.

TABLE 3

Hydrodynamic Pressure on the
Breakwater with Vertical Face

Acceleration a_x (g)	Hydrodynamic Pressure p(psi)			
	y = 18.5 in.	y = 13.25 in.	y = 7.5 in.	y = 2.25 in.
0.185	0.053	0.076	0.082	0.080
0.250	0.035	0.102	0.115	0.098
0.355	0.053	0.102	0.188	0.190
0.420	0.053	0.160	0.203	0.245
0.460	0.058	0.174	0.188	0.290
0.500	0.067	0.188	0.232	0.357
0.835	0.125	0.348	0.522	0.445

(9) Depress the Gilmore Command Selector Function Generator switch.

(10) Trigger the oscilloscope with hand held switch.

(11) Use oscilloscope camera to take pictures for the responses appeared on the Cathode-ray tube of the oscilloscope.

(12) Repeat the above procedures for different accelerations.

(13) Stop the actuator, turn off the power and release the water.

(14) Reconstruct a model breakwater and repeat the above procedures.

3.3 Experimental Results

A. From the experimental data [Appendix 6], the hydrodynamic pressure on the breakwater at each elevation for both models tested were calculated. The results are shown in Tables 3 and 4.

B. Pressure at different elevations against intensity of earthquakes are plotted in Figures 6 and 7. As one would expect, in general, the stronger the earthquake and the deeper the position on the breakwater, the larger the hydrodynamic pressure. A general linear trend is also shown in these experimental results.

TABLE 4

Hydrodynamic Pressure on the Breakwater with 30° Inclined Face

Acceleration a_x (g)	Hydrodynamic Pressure p(psi)			
	y = 18.5 in.	y = 13.25 in.	y = 7.5 in.	y = 2.25 in.
0.148	0.010	0.030	0.052	0.032
0.190	0.012	0.040	0.062	0.049
0.230	0.014	0.052	0.084	0.061
0.250	0.018	0.062	0.095	0.075
0.295	0.022	0.073	0.105	0.105
0.335	0.025	0.084	0.127	0.119
0.375	0.028	0.105	0.138	0.134
0.585	0.043	0.148	0.214	0.192

C. Cumulative deformation of breakwater: as shown in Figure 8 and Table 5, it can be seen that the stronger the earthquake, the larger the slump at the crest of the breakwater. Except the settlement of the crest, there is no significant deformation for acceleration below 0.25 g. When acceleration is larger than 0.25 g, a slight bulging was observed on both faces of the breakwater and an outward displacement was also noted on both toes. As expected, the steeper slope was more sensitive to the motion and the displacement of the rear toe was greater than that of the front toe. There were no holes formed on the Dolosse armor layer during the experiment except some densification of the Dolosse occurred at the bottom of the breakwater while a thinning took place on the crest.

TABLE 5

Data for the Deformation of a Breakwater

α (g)	h_c (in.)	h_f (in.)	h_r (in.)	d_f (in.)	d_r (in.)
0.210	1.0	7.5	8.0	0	0
0.250	2.0	7.75	8.25	0	0
0.335	2.5	7.5	8.75	0	1.0
0.375	3.25	7.25	8.5	0.625	2.5
0.630	5.25	6.875	8.0	1.25	4.5

D. Figure 9 shows the relation between the pressure change on breakwater at the water surface and the intensity of earthquakes. The results seem to indicate that the effect of surface wave becomes larger and irregular as the inclined angle increases. It should be noted that the surface dynamic pressure was assumed to be zero for all the theoretical work in this thesis. This assumption could be in error as much as 0.125 psi as shown in Figure 9.

CHAPTER IV

COMPARISON OF EXPERIMENT WITH THEORY

Comparisons are made among results of the experiments, results obtained from the extended Von Kármán's theory and results of Zangar's experiments.

A. Equivalent Pressure Coefficients from Extended Von Kármán's Theory

From Equations (28) and (30), and the definition that $a_x = \alpha g = \alpha\, w/\rho$, it follows that

$$p = \rho b\, a_x \sin^2\theta = b \sin^2\theta\, \alpha\, w \tag{48}$$

and according to Zangar's definition [5],

$$p = c_p\, \alpha\, w\, h \tag{49}$$

where c_p is the pressure coefficient.

From Equations (48) and (49), it follows that

$$c_p = \frac{b}{h} \sin^2\theta \tag{50}$$

For $\theta = 30°$, $45°$ and $90°$, values of the pressure coefficients are calculated from (50) [Appendix 3] and are compared with Zangar's result as shown in Figure 17.

B. Equivalent Pressure Coefficients from the Experimental Results

Since $p = c_p \alpha w h$, then for the total water depth h = 18.5 in.,

$$c_p = \frac{1}{wh} \frac{p}{\alpha} = \frac{1728}{62.4 \times 18.5} \frac{p}{\alpha} = 1.4968 \frac{p}{\alpha} \qquad (51)$$

For any elevation on the breakwater, c_p are calculated [Appendix 4] for different values of the acceleration coefficient α and the corresponding pressure change, p. The ensemble averages and the standard deviations are also calculated in Appendix 4.

C. Comparison of Pressure Coefficients from Sections A and B with Zangar's Results

Three curves representing pressure coefficients from Sections A, B and Zangar's results, respectively, are plotted together in Figure 10 and Figure 11 for a breakwater with vertical front face and 30° inclined surface, respectively.

It can be seen from the figures that these three curves are close to one another for the breakwater with vertical front face except that the pressure coefficient representing our experiment is not zero on the water surface. This is caused by the surface wave. Though it is not too significant, the effect of surface wave becomes larger and larger as the horizontal acceleration increases.

For the breakwater with a 30° inclined surface, the three curves are separated apart from one another. It seems to reflect

the effect of the greater degree of idealization in the theoretical results in this case. The effect of surface wave is shown in Figure 9 to be smaller than that of the breakwater with vertical face.

D. As shown in Figure 12, a comparison is made to study this relation between the pressure coefficient at the bottom and the inclined angle of the breakwater. It is apparent that Zangar's result is closer to the extended Von Kármán's theory than our experiment. A fairly good agreement is shown between the results from Zangar's experiments and the extended Von Kármán's theory. Our experimental curve deviates from the other two curves considerably for $\theta > 45^{o}$. For $\theta < 45^{o}$, all three curves show fairly good agreement.

CHAPTER V

CONCLUSIONS AND RECOMMENDATIONS FOR FURTHER STUDIES

A. Conclusions

(1) The hydrodynamic pressure on the breakwater at water surface is not zero due to horizontal earthquake and the stronger the earthquake, the larger the hydrodynamic pressure.

(2) The approximate solution of Von Kármán agrees with experiments for the breakwater with a vertical face. For the breakwater having a face of large inclined angle, an approximate solution from the extended Von Kármán's theory deviates considerably from the experimental result. It should be noted that the solution obtained from the extended Von Kármán's theory is solved for the steady-state while the input loading of the experiment is an impulse force. In addition, two dimensional conditions were assumed in the Von Kármán's theory while actually three dimensional conditions were involved in the experiment.

(3) From experiments, the maximum pressure is found at some distance above the bottom of the breakwater with 30° inclined face while it was found at the base of the breakwater having a vertical face.

(4) The maximum value of pressure coefficient is found from an experiment to be 0.835 at the base of a breakwater having a vertical face, while those from the analytic solution of Von Kármán and the experimental analog solution of Zangar are, respectively, 0.72 and 0.735.

(5) In the experiments, the surface wave generated by the breakwater with a vertical face is larger than that of the breakwater with a 30° inclined face.

(6) For earthquake intensities less than about 0.35 g, except for a slight settlement at the crest, there is no significant deformation for the breakwater. So it appears that a rubble-mound breakwater has a great deal of strength to resist earthquakes.

(7) The extended Von Kármán's theory shows a good approximation of Westergaard's solution. On the bottom of the breakwater, the difference between the maximum dynamic pressure from Westergaard's solution and the dynamic pressure calculated from extended Von Kármán's theory is about 4 or 5 percent.

B. Recommendations for Further Studies

(1) In experiments, the effect of the reflection of waves in the front and the absorption of waves in the back of the breakwater should be further investigated.

(2) Four pressure transducers should be used in each test of the experiment to get better results. Since there were only two transducers available, it was necessary to build two models and run twice to complete a test. It thus induced additional work and caused additional errors. Hence, at least to have two more pressure transducers is suggested.

(3) The model breakwater used in the experiment was constructed not completely according to the prototype breakwater because of the various constraints in time and facilities. In order to study the behavior of a prototype breakwater, it will be necessary to improve the model based on the scaling theory.

(4) For the purpose of decreasing the disturbance near the edge of the shake table, a larger scaled shake table is recommended so that the experimental situation will be much closer to that of the prototype.

(5) Tests of breakwaters with a vertical face and breakwaters with a 30° inclined face were conducted in this experiment. It shall be informative to run more tests for the breakwater with 45° and 60° inclined faces so that a series of curves can be plotted and compared to each other.

(6) The pressure changes were only measured on the front face of the breakwater in the experiment. It is suggested to measure the

pressure changes on both sides of the breakwater. Then the pressure increase and decrease on both sides of the breakwater can be measured from which the stability of the breakwater during the earthquake can be better estimated.

(7) For theoretical studies, an "exact" solution for hydrodynamic pressure on a breakwater with an inclined face should be sought for as the next improvement over the approximate solution base on the extended Von Kármán's theory. This may proceed in two steps: (i) without surface wave effects and (ii) with surface wave effects included.

(8) A practical result is suggested to be obtained from the analytical solution so that it can be compared with the experimental result. A solution for the transient-state in the theoretical analysis and results for steady-state in the experiment are also recommended.

REFERENCES

1. Westergaard, H. M., "Water Pressures on Dams During Earthquakes," Trans., ASCE, Vol. 98, 1933.

2. Von Kármán, T., Discussion of "Water Pressures on Dams During Earthquakes," Trans., ASCE, Vol. 98, 1933.

3. Brahtz, H. A. and Heilbron, C. H., Discussion of "Water Pressures on Dams During Earthquakes," Trans., ASCE, Vol. 98, 1933.

4. Werner, P. W. and Sundquist, K. J., "On Hydrodynamic Earthquake Effects," Trans., American Geophysical Union, Vol. 30, No. 5, Oct., 1949.

5. Zangar, C. N., "Hydrodynamic Pressures on Dams Due to Horizontal Earthquakes," Proc., SESA, Vol. 10, No. 2, 1953.

6. Chen, C. C., "The Effect of Dynamic Fluid Pressure on a Dam During Earthquakes," J., PMM, Vol. 25, No. 1, 1961.

7. Chopra, A. K., "Hydrodynamic Pressures on Dams During Earthquakes," Proc., ASCE, Vol. 90, EMG, Dec., 1967.

8. Lamb, H., "Hydrodynamics," Dover, 1945.

9. Wang, H., Chen, S. S., and Yang, C. Y., "Water Pressures on Rubble-Mound Breakwater Due to Earthquakes," Abstract published in Proc. of Specialty Conf. on Mechanics of Engineering, ASCE-EMD, Univ. of Waterloo, Canada, May, 1976.

10. Ince, E. L., "Ordinary Differential Equations," Dover, 1956.

11. Lin, Y. K., "Probabilistic Theory of Structural Dynamics," McGraw-Hill, 1967.

12. Campbell, G. A. and Foster, R. M., "Fourier Integrals for Practical Applications," D. Van Nostrand, 1948.

13. Clough, R. W. and Penzien, J., "Dynamics of Structures," McGraw-Hill, 1975.

14. Lamison, C., "Response of Rubble-Mound Breakwater to Earthquake Loads," Master Thesis, Dept. of Civil Engrg., Univ. of Delaware, 1976.

APPENDIX 1

A. Calibration of the Accelerometer

The accelerometer was mounted on the shake table to which a horizontal earthquake motion was imposed (see Photograph 4). The accelerometer was dynamically calibrated by an Instron, Model 306-10, actuator, as shown in Photograph 8, which is a precision unit, engineered for reliable operation in Servo-hydraulic systems in the Mechanical Testing Lab of the Department of Mechanical and Aerospace Engineering.

A sinusoidal motion was generated with a frequency of 2.5 cycles per second. The amplitude was changed to simulate the variation of acceleration.

Through a Vishay, Model BAM-1, bridge amplifier meter, a two-channel chart-recorder and a volt meter were connected to the accelerometer. The volt meter was used to keep the excitation of the accelerometer to be excatly 11 volts and the two-channel chart-recorder was used to record the response of the accelerometer.

The calibration result was shown in Figure 13.

B. Calibration of the Pressure Transducers

A loop as shown in Figure 14 was arranged to calibrate the pressure transducers.

The shut-off valve was opened to let the air in and the bleed valve was completely opened at the beginning of the calibration and then slowly closed to increase the pressure. Thus, the transducer output voltage was gradually increased. The output voltage on the volt meter was then read with the selected pressure recorded on the pressure gauge.

The pressure-voltage relation for both pressure transducers were shown in Figures 15 and 16 respectively.

APPENDIX 2

CALIBRATION OF OSCILLOSCOPE

In order to ensure correct calibration, it should be noted that any time one moves the Type 3A74 amplifier from one oscilloscope plug-in opening to another, the common gain of the unit must be readjusted to compensate for differences in CRT deflection sensitivities. The calibration procedures are as follows:

(1) Set the front-panel controls of the Type 3A74 to the following readings:

AC-GND-DC (Channel 1)	DC
VOLTS/DIV. (Channel 1)	.02
VAR. GAIN (Channel 1)	CAL
POSITION (Channel 1)	Centered
MODE (Channel 1)	NORM
MODE (Channels 2,3 and 4)	OFF

(2) Set the time-base sweep rate and triggering controls for an 0.1 ms/div free running sweep.

(3) Apply an 0.1-volt signal from the oscilloscope calibrator to the Channel 1 connector by using a short test lead through a suitable connector adapter to make the direct connection.

(4) Adjust the calibration control to obtain a deflection on CRT of exactly five major divisions.

APPENDIX 3

CALCULATION OF THE EQUIVALENT PRESSURE COEFFICIENTS FOR EXTENDED VON KARMAN THEORY

A. For $\theta = 90°$, from Equation (34), it gives

$$k^2 = 2\,h^2$$

substituting into (33), it yields

$$b = 0.707\sqrt{h^2 - y^2}$$

then from Equation (50), it follows

$$c_p = 0.707\sqrt{1 - \left(\frac{y}{h}\right)^2} \qquad (52)$$

Hence, for an arbitrary elevation y, the pressure coefficient c_p can be found from (52).

B. For $\theta = 30°$, from Equations (34) and (33), it follows

$$k^2 = 0.7281\,h^2$$

$$\left|\frac{2y^2 - by + 2b}{0.7281\,h^2}\right| = \exp\{0.6433\,\tan^{-1}\,[1.4856\,\frac{y}{b} - 0.3216]\} \qquad (53)$$

then from (50), it gives

$$c_p = 0.25 \frac{b}{h} \tag{54}$$

Equation (53) was then solved as in Table 6, in which the pressure coefficient c_p was calculated from Equation (52).

TABLE 6

Calculation of Equivalent Pressure Coefficient for Breakwater with a 30° Inclined Face from Extended Von Kármán's Theory

$\frac{y}{b}$	$\text{Exp}\{0.6433 \tan^{-1} [1.4845 \frac{y}{b} - 0.3216]\}$	$\frac{2y^2 - by + 2b^2}{0.7281 h^2} = ? \frac{b^2}{h^2}$	$\frac{b}{h}$	$\frac{y}{h}$	c_p
0	.8186	2.7469	.5459	0	.1365
.1	.8956	2.6370	.5828	.0583	.1457
.2	.9844	2.5821	.6174	.1235	.1544
.3	1.0827	2.5821	.6475	.1943	.1619
.5	1.2923	2.7469	.6859	.3430	.1715
.8	1.5832	3.4061	.6822	.5458	.1706
1.0	1.7400	4.1203	.6499	.6499	.1625
1.2	1.8671	5.0543	.6078	.7294	.1519
1.5	2.0133	6.8672	.5415	.8122	.1354
2.0	2.1778	10.9872	.4452	.8904	.1113
3.0	2.3581	23.3484	.3178	.9534	.0794
10.0	2.6282	263.7000	.0998	.9983	.0250

C. For $\theta = 45°$, from Equations (34) and (33), it follows

$$k^2 = 0.8887\ h^2$$

$$\left|\frac{2y^2 - by + 2b^2}{.8887\ h^2}\right| = \exp\{0.5163\ \tan^{-1}[1.0328\ \frac{y}{b} - 0.2582]\} \qquad (55)$$

then from (50), it gives

$$c_p = 0.5\ \frac{b}{h} \qquad (56)$$

Equation (55) was then solved as in Table 7, in which the pressure coefficient c_p was calculated from Equation (56).

TABLE 7

Calculation of Equivalent Pressure Coefficient for Breakwater with a 45° Inclined face from Extended Von Kármán's Theory

$\frac{y}{b}$	$\text{Exp}\{0.5163\ \tan^{-1}[1.0328\ \frac{y}{b} - 0.2582]\}$	$\frac{2y^2 - by + 2b^2}{0.8887\ h^2} = ?\ \frac{b^2}{h^2}$	$\frac{b}{h}$	$\frac{y}{h}$	c_p
.3	1.0267	2.1157	.6966	.2090	.3483
.5	1.1394	2.2507	.7115	.3558	.3558
.8	1.3057	2.7909	.6840	.5472	.3420
1.0	1.4054	3.3761	.6452	.6452	.3226
1.2	1.4927	4.1413	.6004	.7205	.3002
1.5	1.6011	5.6268	.5334	.8001	.2667
2.0	1.7334	9.0029	.4388	.8776	.2194
3.0	1.8893	19.1290	.3143	.9427	.1572
10.0	2.1381	216.0459	.0995	.9950	.0498

APPENDIX 4

A. Calculation of the Equivalent Pressure Coefficients for the Experimental Results

From Equation (51), $c_p = 1.4968\ p/\alpha$. With the experimentally obtained input acceleration coefficient, α, and output pressure, p, c_p were calculated as shown in Table 8 and Table 9.

(1) For $\theta = 90°$

TABLE 8

Equivalent Pressure Coefficients for Breakwater with a Vertical Face

α	c_p			
	y = 18.5 in.	y = 13.25 in.	y = 7.5 in.	y = 2.25 in.
.185	.4286	.6168	.6633	.6472
.250	.2095	.6106	.6885	.5867
.335	.2367	.4556	.8398	.8488
.420	.1887	.5701	.7234	.8730
.460	.1885	.5660	.6115	.9435
.500	.2005	.5627	.6945	1.0687
.835	.2240	.6237	.9356	.7976
Σ	1.6765	4.0055	5.1566	5.7655
ave.	.2395	.5722	.7365	.8236

(2) For $\theta = 30°$

TABLE 9

Equivalent Pressure Coefficients for the Breakwater with a 30° Inclined Face

α	c_p			
	y = 18.5 in.	y = 13.25 in.	y = 7.5 in.	y = 2.25 in.
.148	.1010	.3023	.5258	.3236
.190	.0944	.3150	.4884	.3858
.230	.0910	.3382	.5466	.3969
.250	.1077	.3712	.5687	.4490
.295	.1115	.3703	.5327	.5327
.335	.1115	.3752	.5672	.5316
.375	.1116	.4189	.5506	.5348
.585	.1110	.3785	.5475	.4912
Σ	.8388	2.8696	4.3275	3.6456
ave.	.1048	.3587	.5409	.4557

B. The Ensemble Averages and the Standard Deviations of the Pressure Coefficients

The ensemble averages and the standard deviations of the pressure coefficients for the experimental results were calculated as in Table 10.

TABLE 10

Ensemble Averages and Standard Deviations of Pressure Coefficients for the Experimental Results

Elevation y (in.)	18.5		13.25		7.5		2.25	
Inclined Angle θ (D)	90	30	90	30	90	30	90	30
Ensemble Average of Pressure Coefficient $\langle c_p \rangle$	.2395	.1048	.5722	.3587	.7365	.5499	.8236	.4557
Standard Deviation of Pressure Coefficient σ_c	.0738	.0078	.0498	.0355	.1039	.0242	.1537	.0750

APPENDIX 5

PHOTOGRAPHS

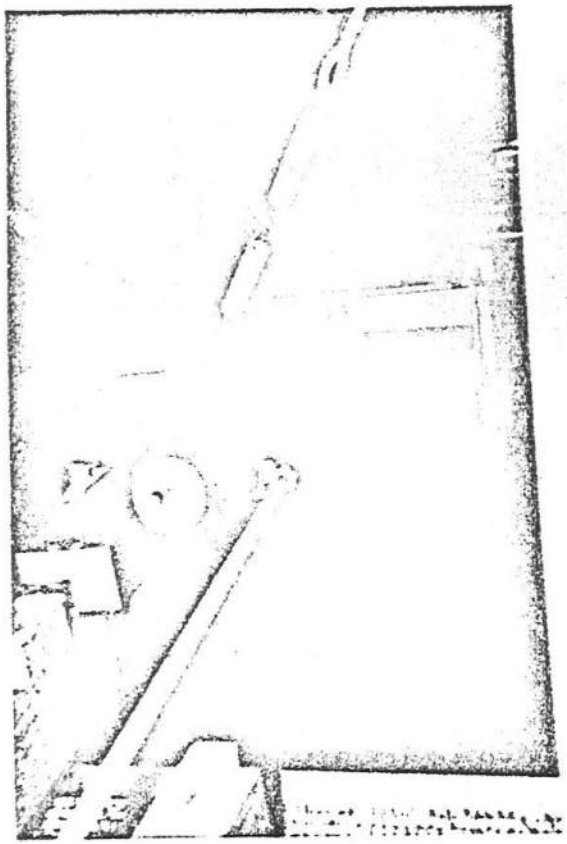

Photograph 1 Model in Wave Tank-Loading End (Back Face at Bottom of Photograph).

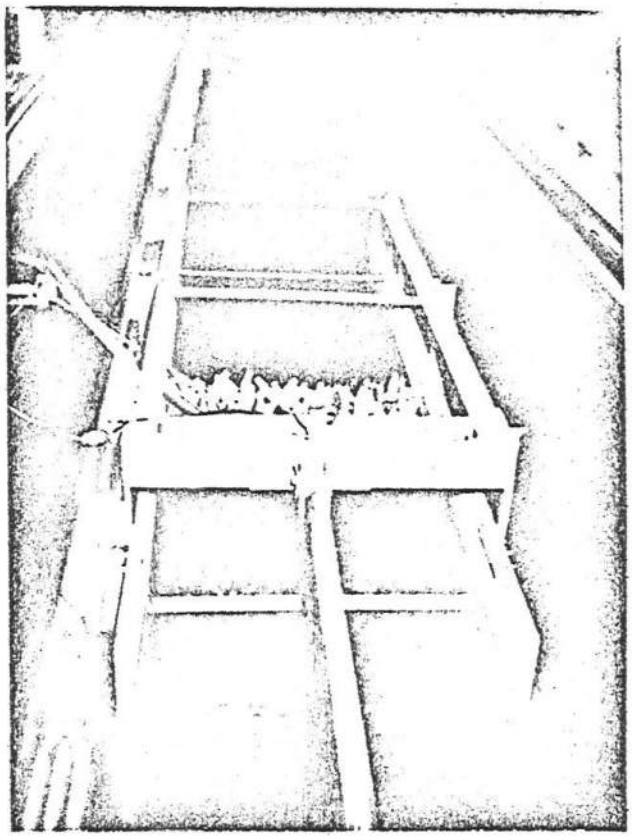

Photograph 2 Model in Wave Tank-Front at the Top of Photograph.

Photograph 3 Location of the Accelerometer

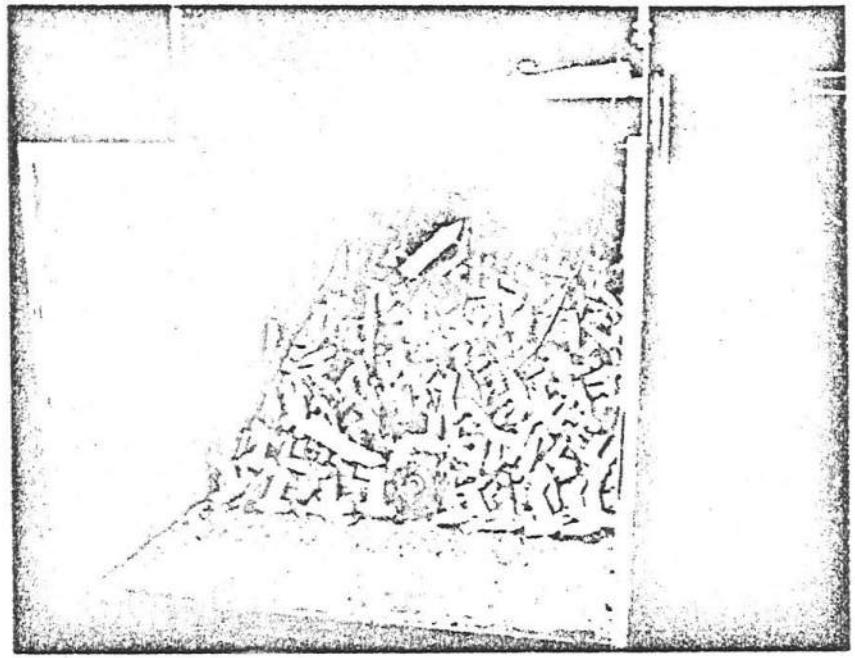

Photograph 4 Locations of the Two Pressure Transducers (Pointed by Arrowheads).

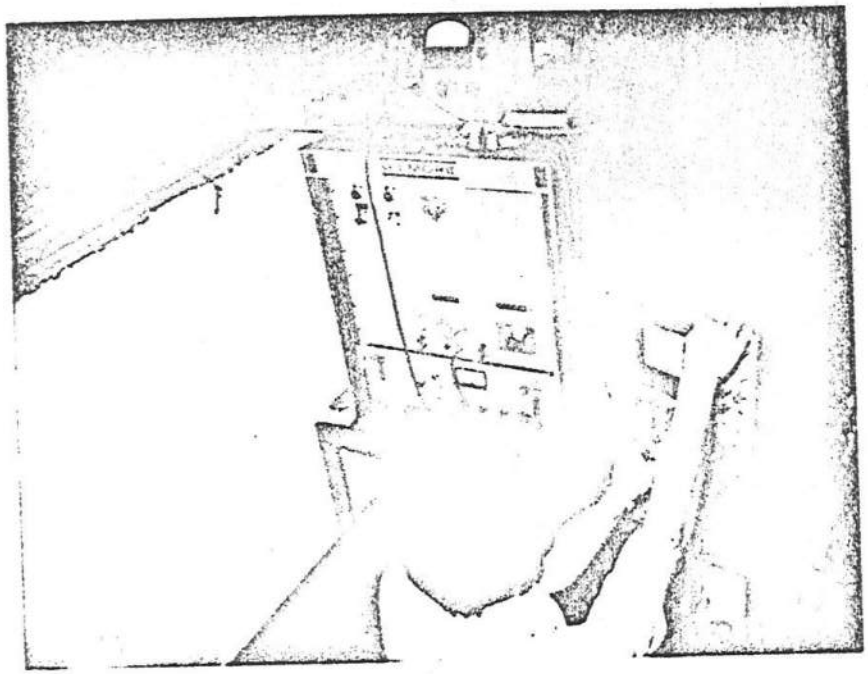

Photograph 5 Connection of (1) Accelerometer, BAM-1, and Oscilloscope and (2) Pressure Transducer, Amplifier (Viatran, Model 601), and Oscilloscope.

Photograph 6 Calibration of Accelerometer

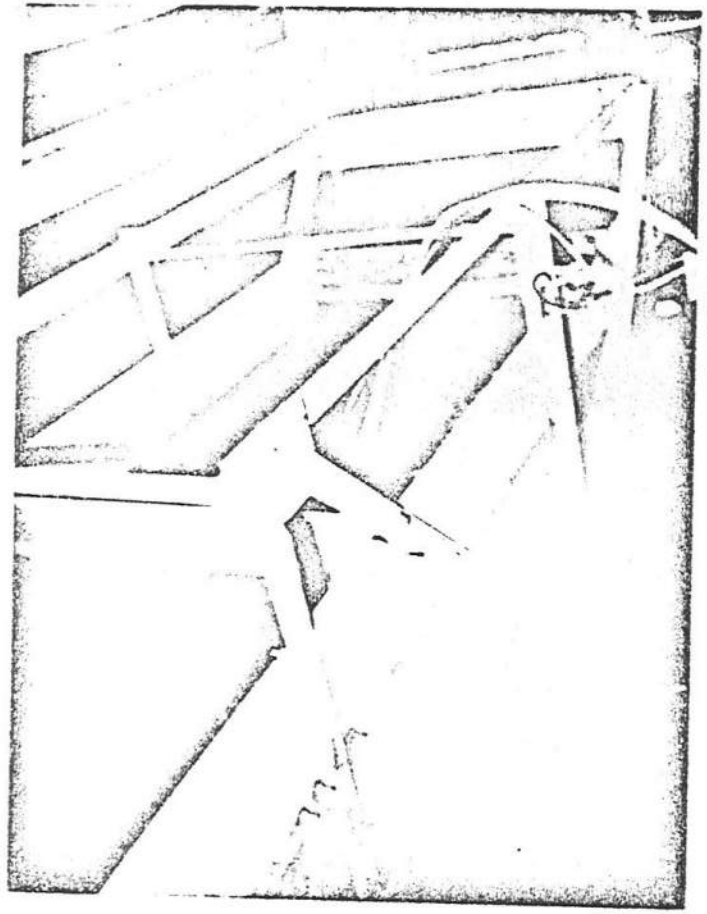

Photograph 7 Breakwater with Vertical Faces

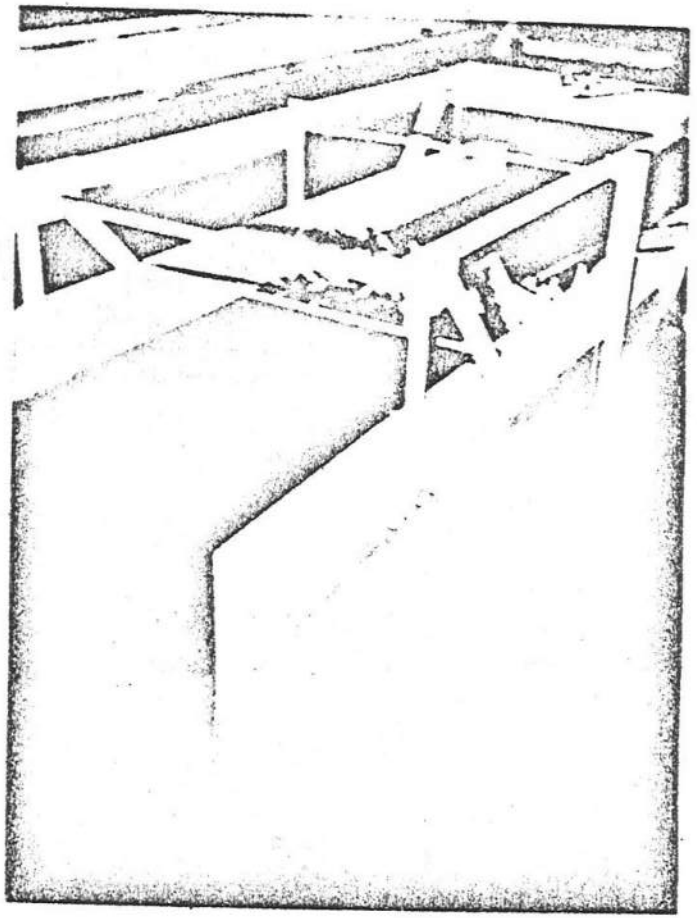

Photograph 8 Breakwater with Inclined Faces

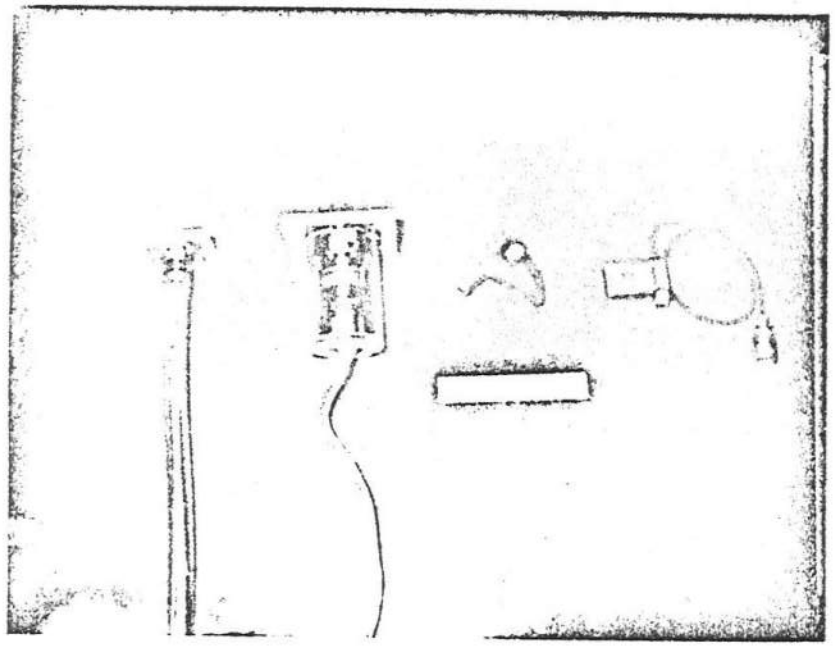

Photograph 9 (LEFT) Pressure Transducer, Statham Model 131; (MIDDLE LEFT) Pressure Transducer, Viatran, Model 103; (MIDDLE RIGHT) Model Dolos; (RIGHT) Accelerometer, Statham, Model A5

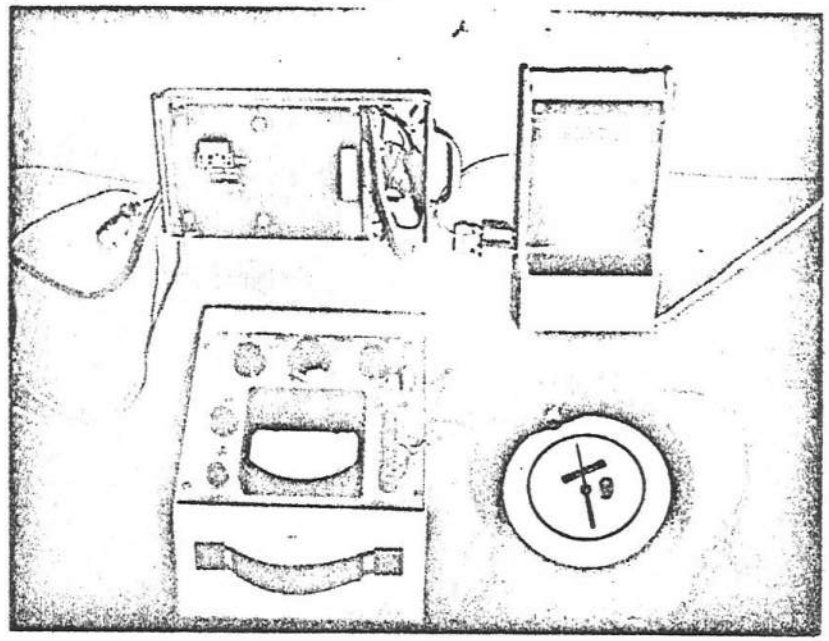

Photograph 10 (UPPER LEFT) Heise, Solid Front-CMM-2642, Pressure Gauge; (UPPER RIGHT) Vishay, Model BAM-1, Bridge Amplifier Meter; (LEFT) Tekelect, Model TA357, Volt Meter; (RIGHT) D.C. Regulated Power Supply

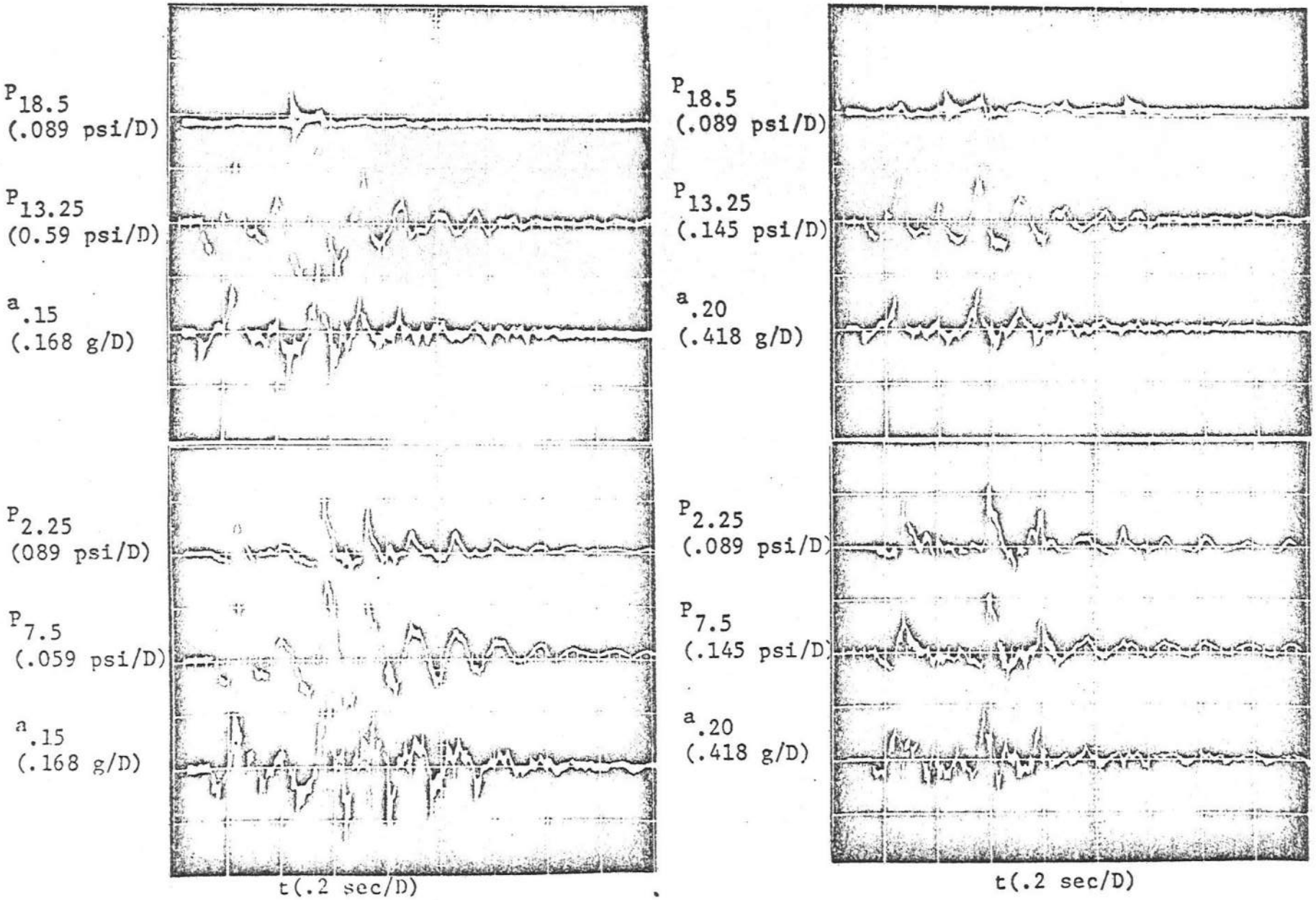

Photograph 11. Output Data for Breakwater with a Vertical Face (A = .15 in., .20 in.)

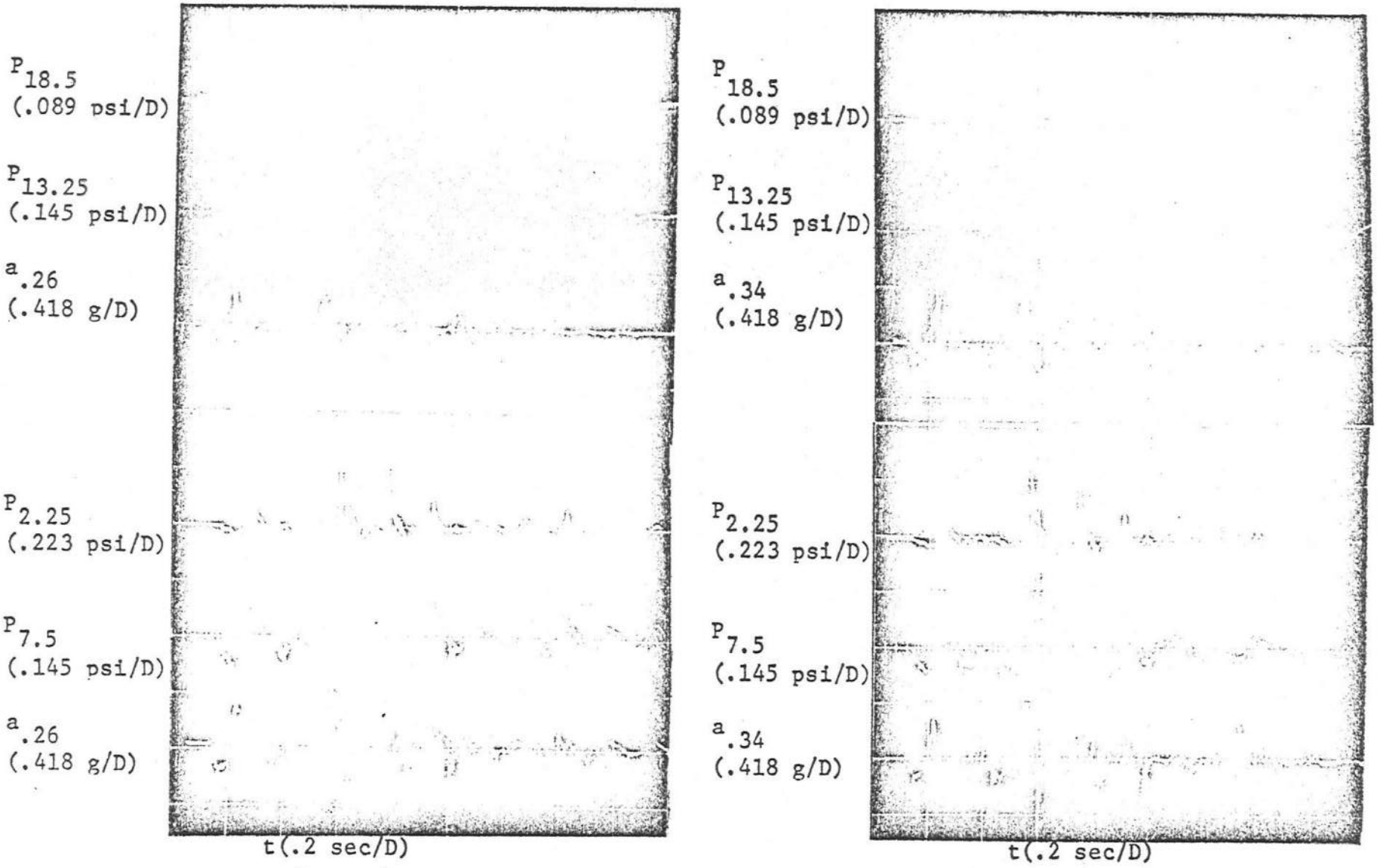

Photograph 12 Output Data for Breakwater with a Vertical Face (A = .26 in., .34 in.)

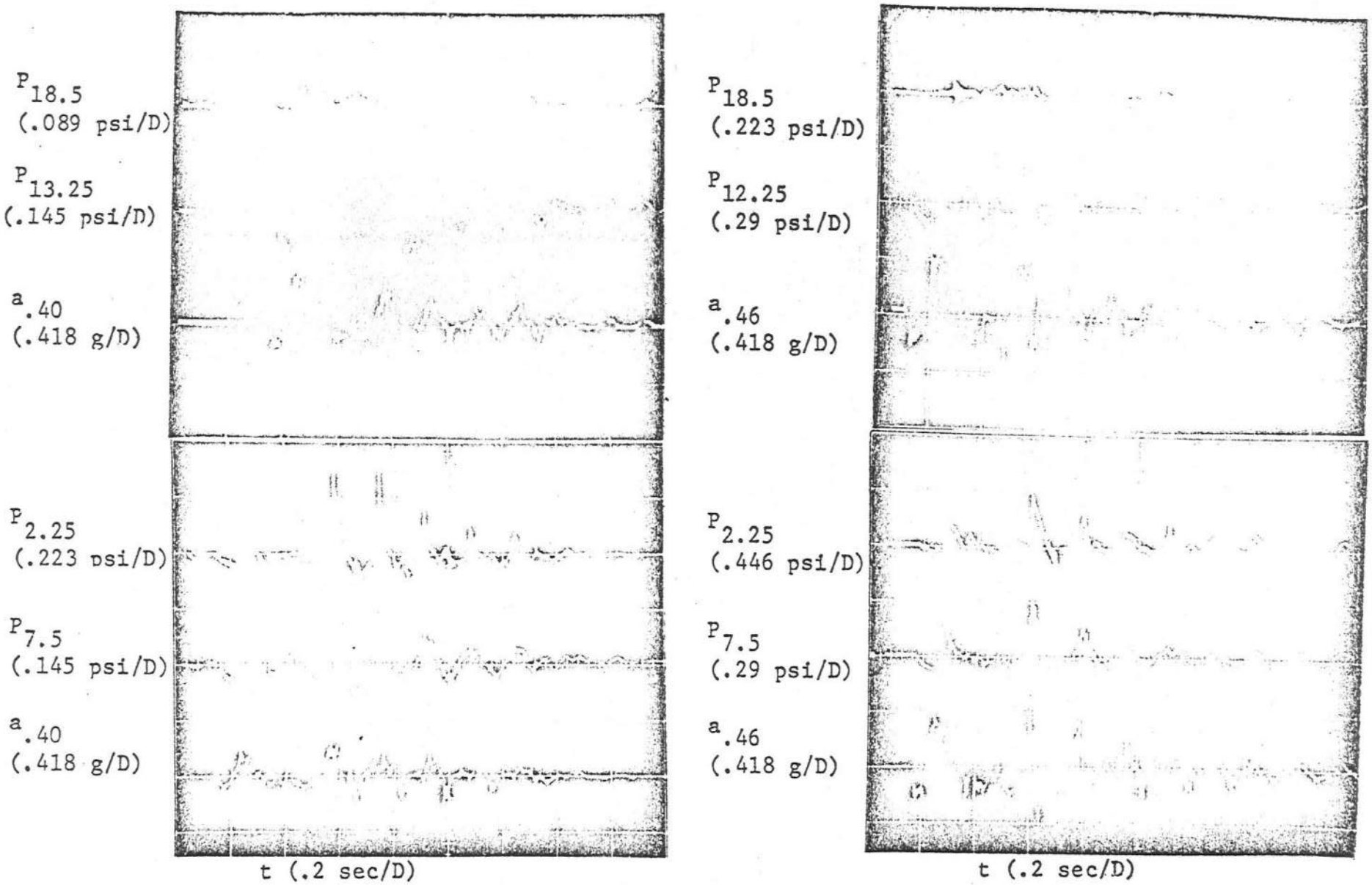

Photograph 13 Output Data for Breakwater with a Vertical Face (A = .40 in., .46 in.)

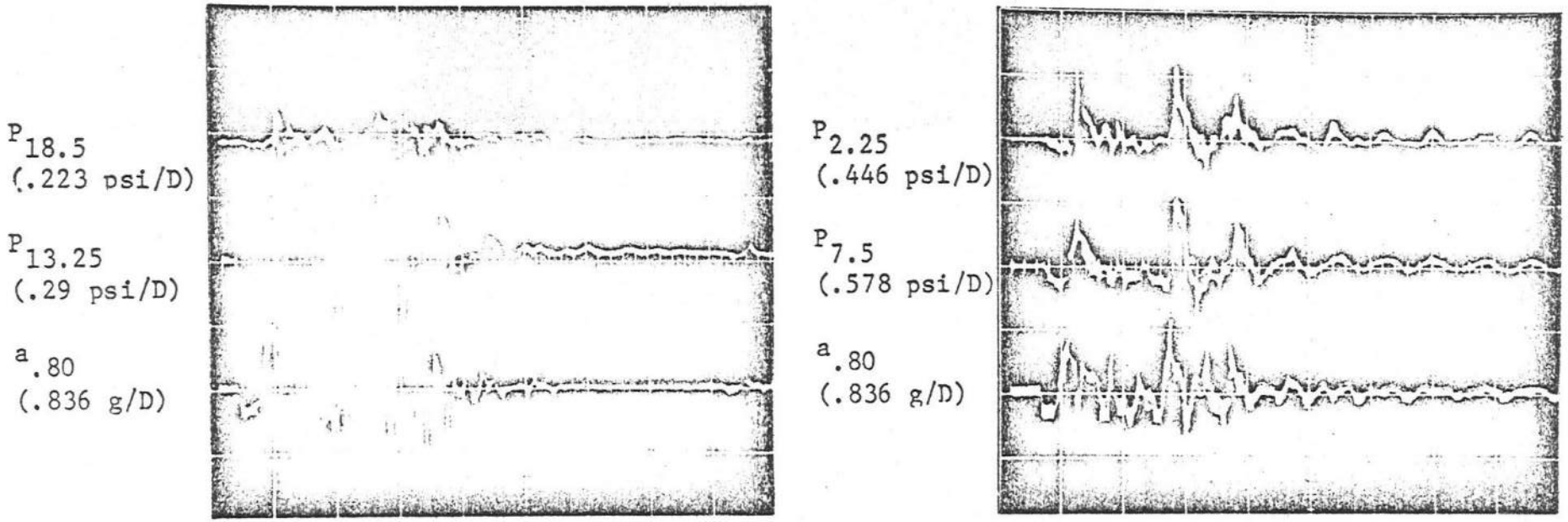

Photograph 14 Output Data for Breakwater with a Vertical Face (A = .80 in.)

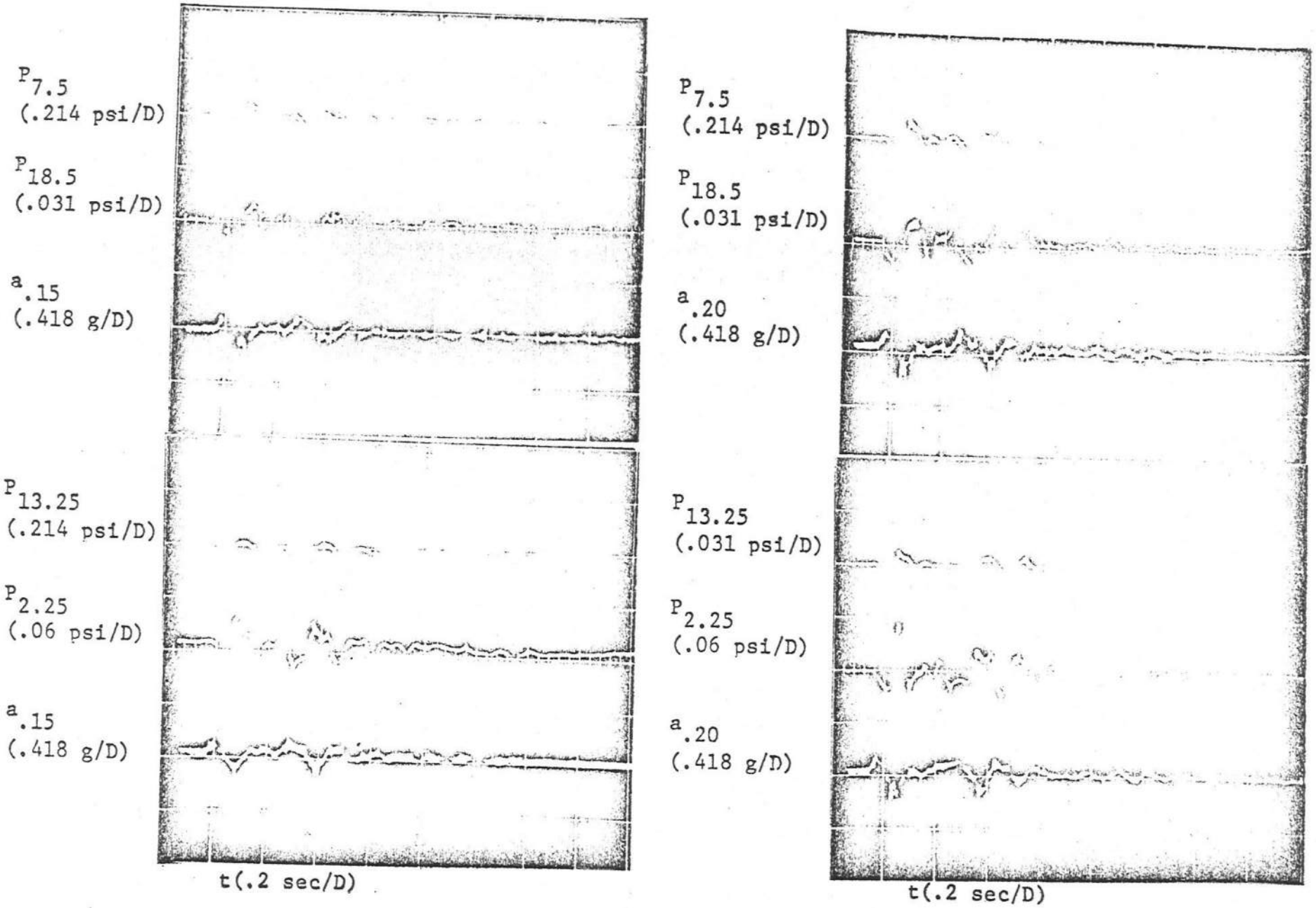

Photograph 15 Output Data for Breakwater with a 30° Inclined Face (A = .15 in., .20 in.)

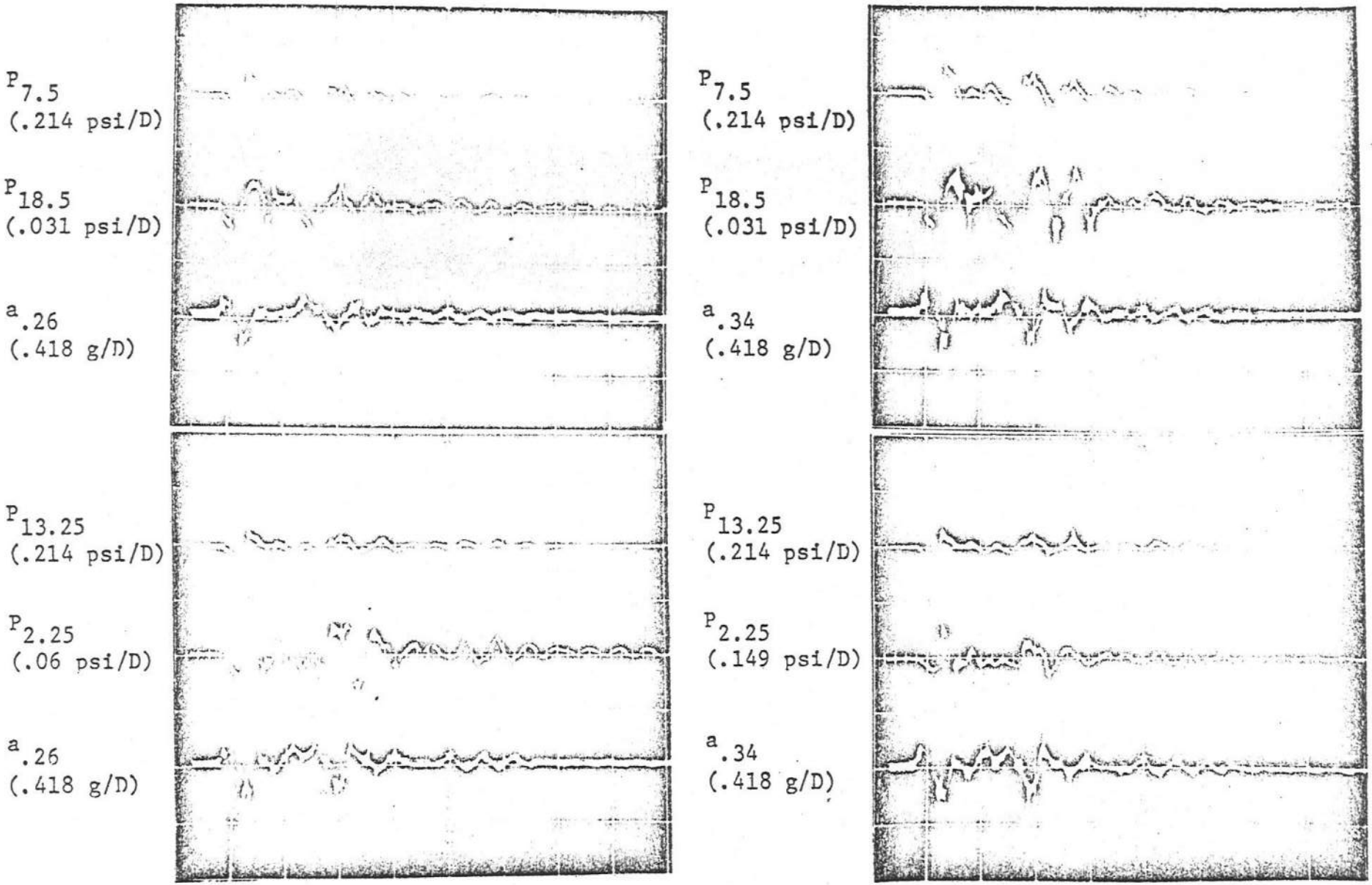

Photograph 16 Output Data for Breakwater with a 30° Inclined Face (A = .26 in., .34 in.)

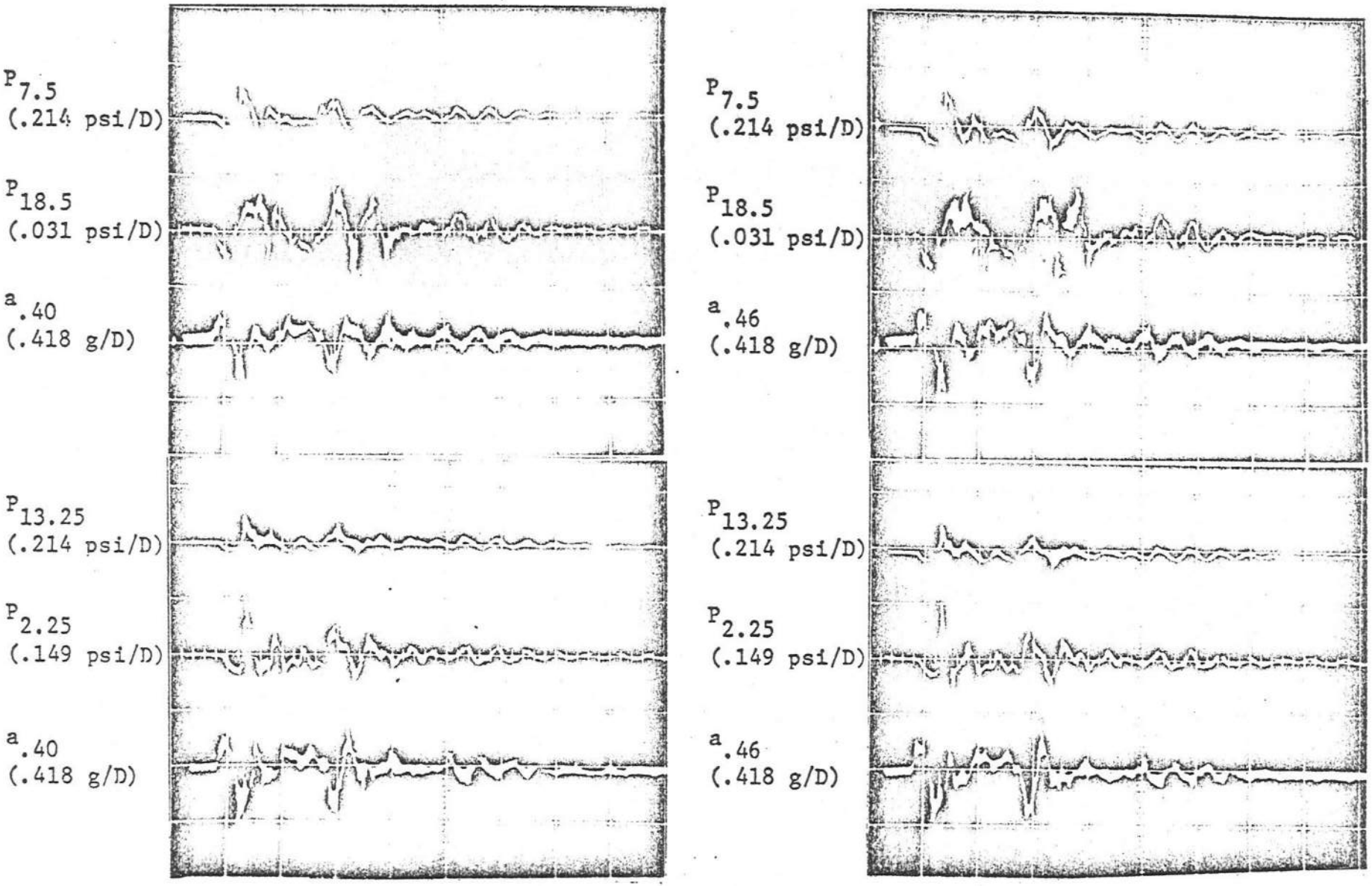

Photograph 17 Output Data for Breakwater with a 30° Inclined Face (A = .40 in., .46 in.)

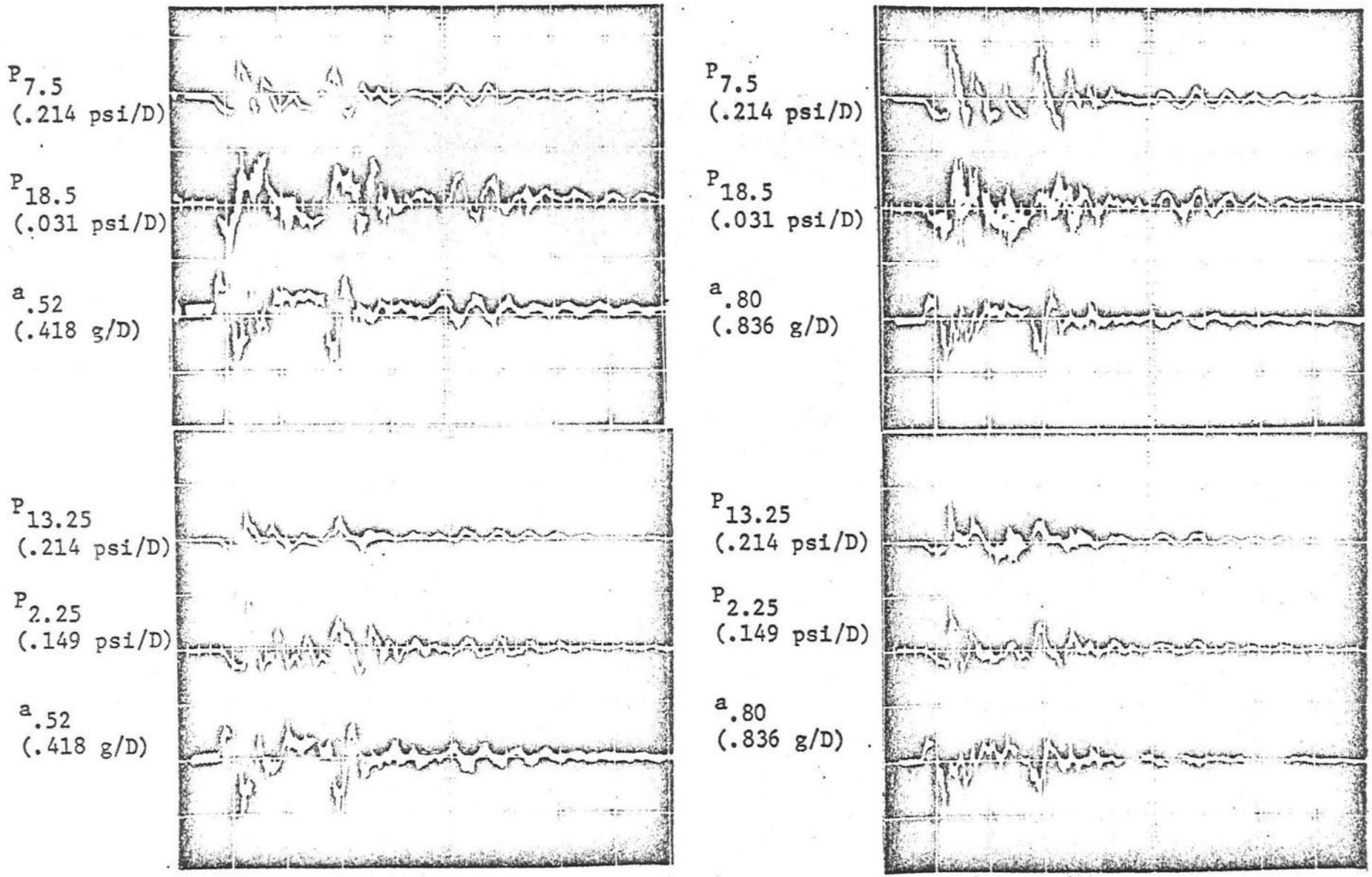

Photograph 18 Output Data for Breakwater with a 30° Inclined Face (A = .52 in., .80 in.)

APPENDIX 6

Output Data of the Experiment

Conventions:

1. P_y is the hydrodynamic pressure on the face of the breakwater at elevation y (in.) from the bottom.

2. a_A is the acceleration corresponding to the amplitude A (in.) of the motion generated.

3. t is time.

4. D means division (or 5 subdivision).

APPENDIX 7

FIGURES

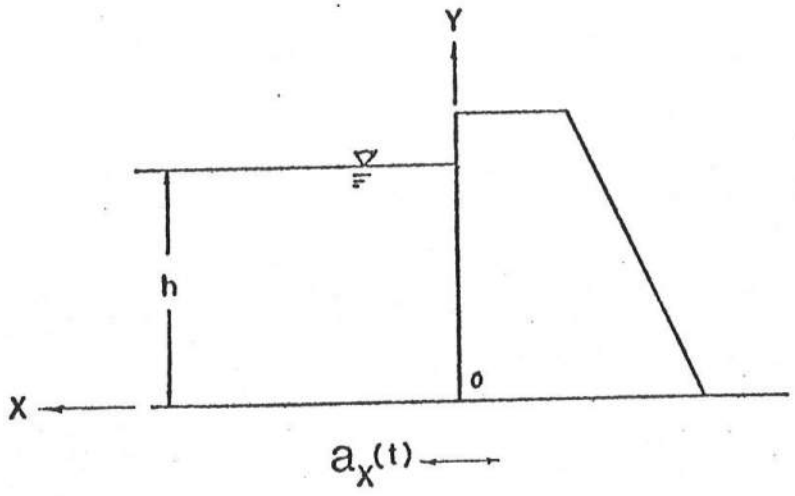

FIGURE 1 A Rigid Breakwater with a Vertical Front Face

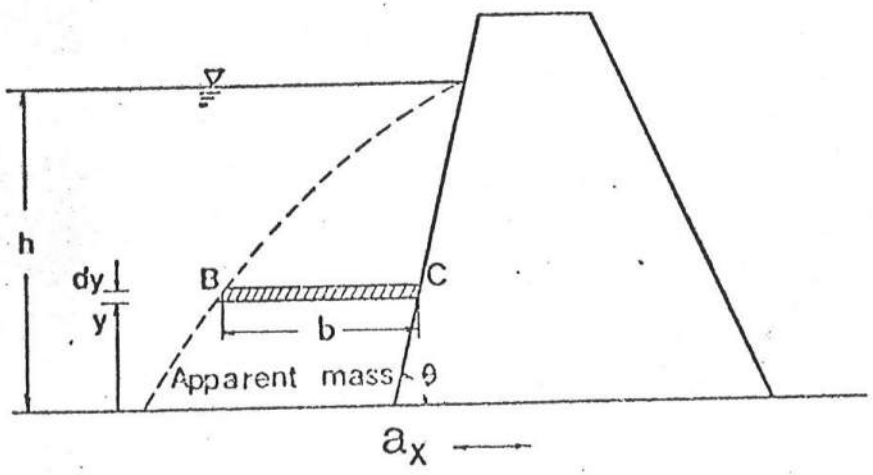

FIGURE 2 A Breakwater with an Inclined Front Face

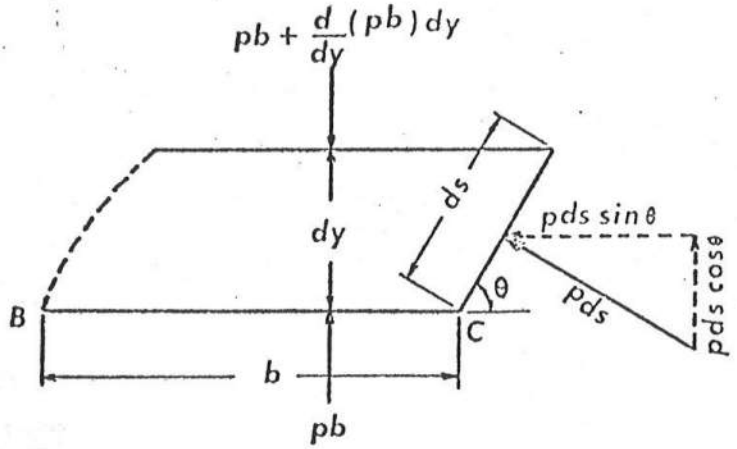

FIGURE 3 Equilibrium of Forces on a Fluid Element

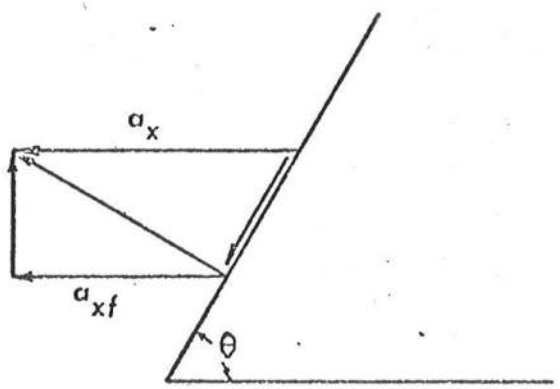

FIGURE 4 Boundary Condition on the Inclined Front Face

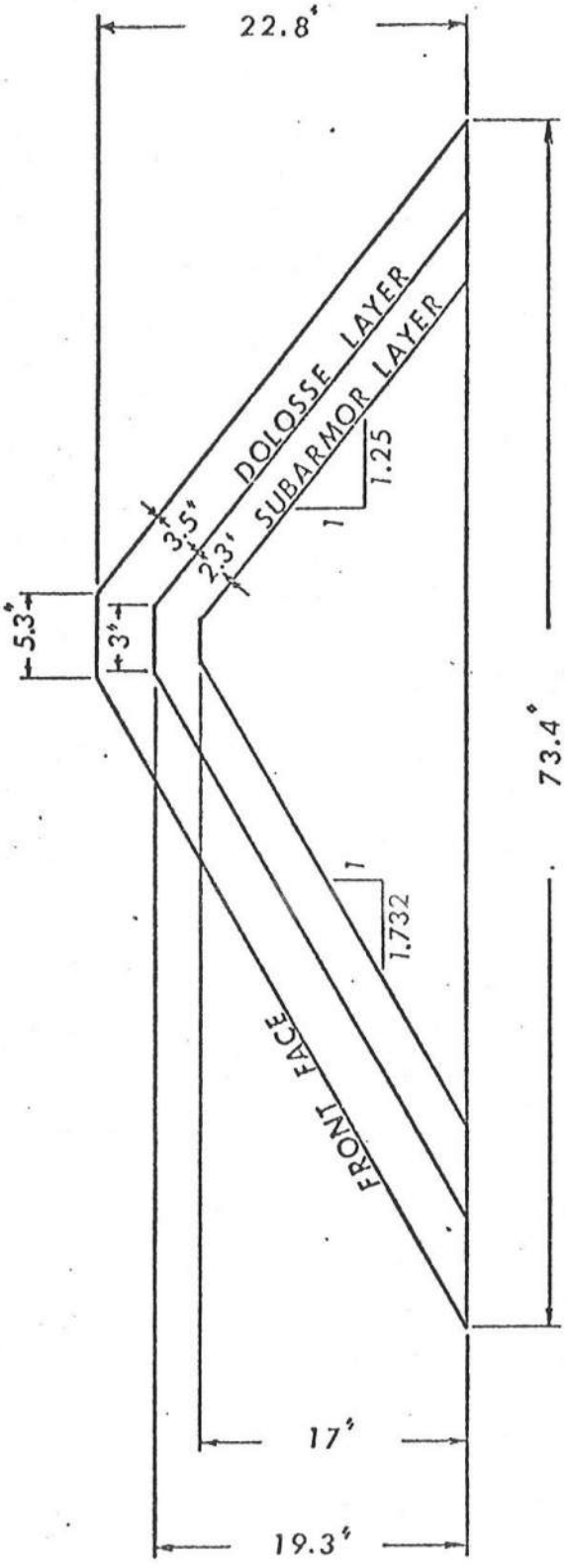

FIGURE 5 Dimensions of the Model Breakwater

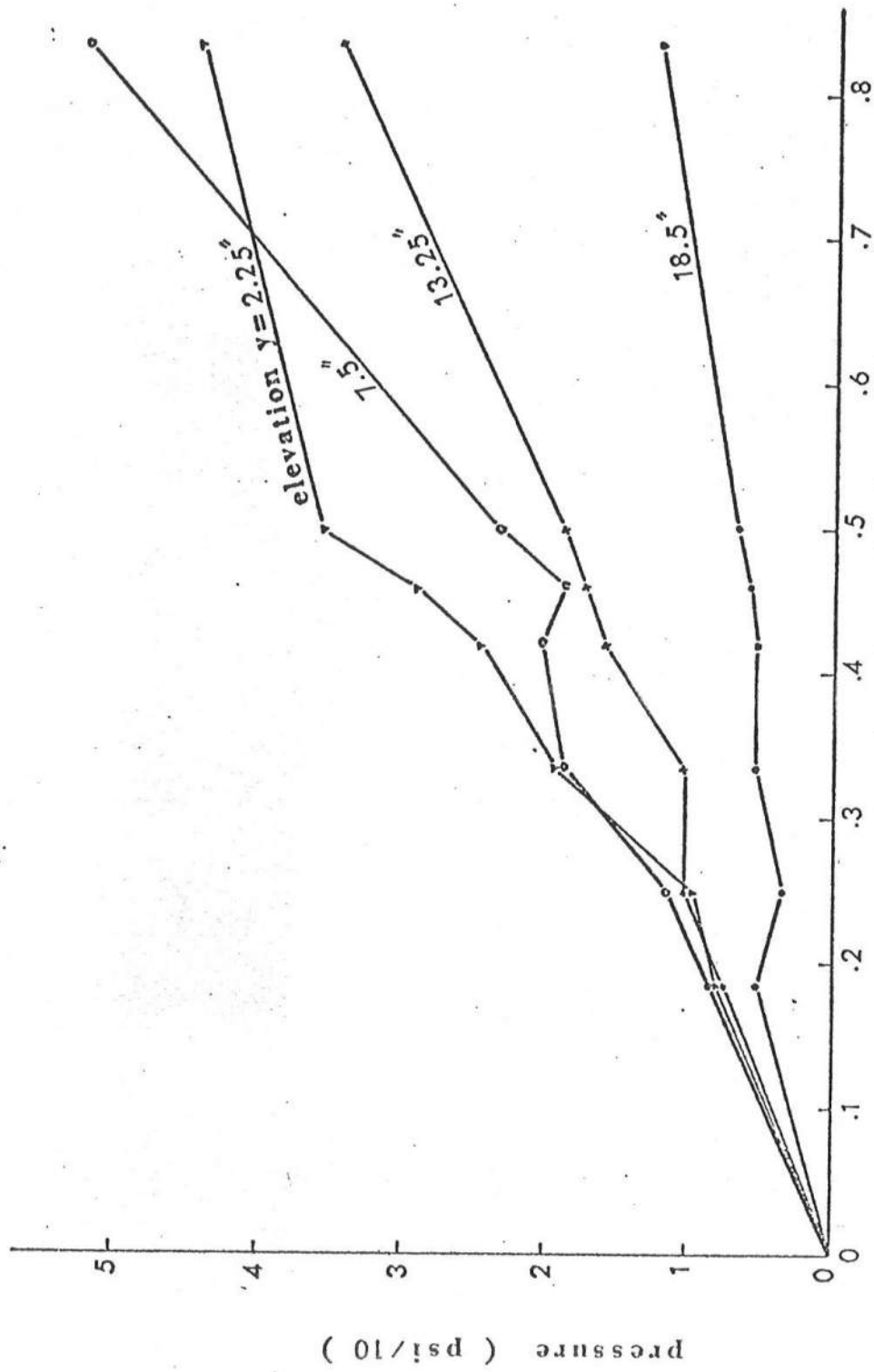

FIGURE 6 Hydrodynamic Pressure at Difference Elevations vs. Ground Accelerations for the Breakwater with a Vertical Face

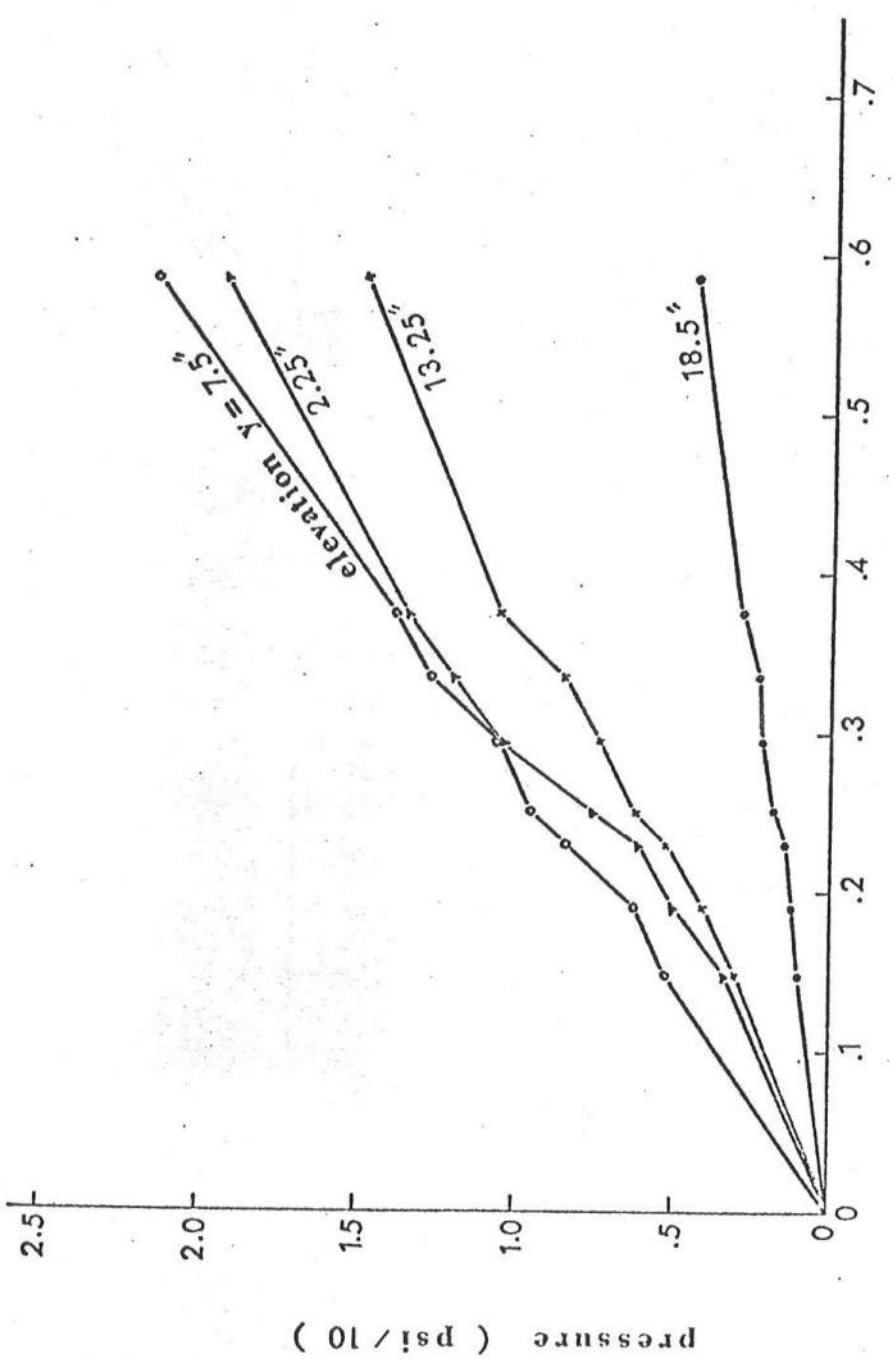

FIGURE 7 Hydrodynamic Pressure at Different Elevations vs. Ground Accelerations for the Breakwater with a 30° Inclined Face

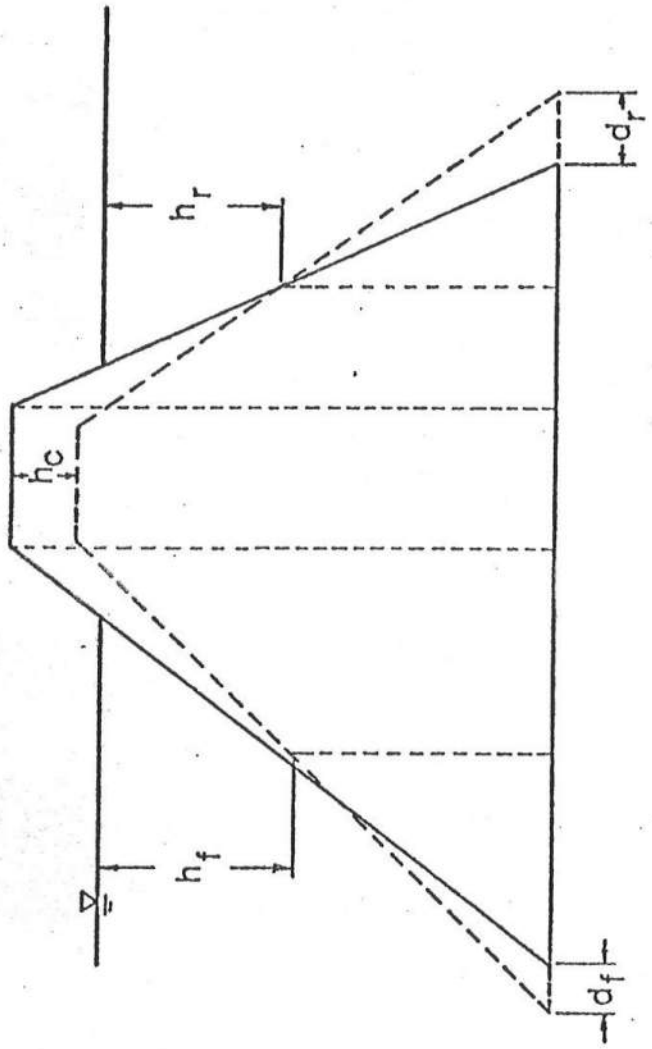

FIGURE 8 Deformed Profile of a Breakwater

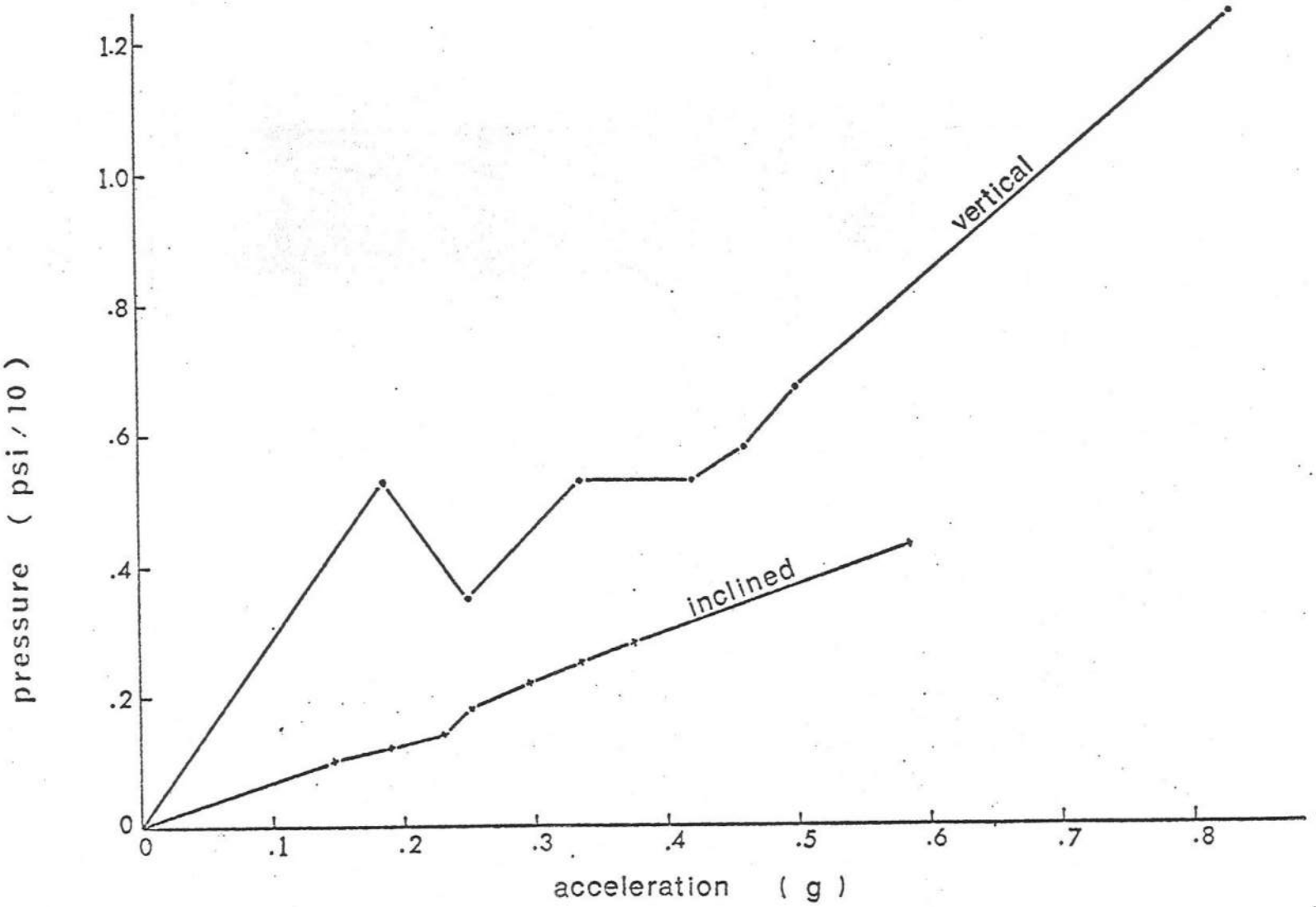

FIGURE 9 Surface Wave Effect: Pressure on the Breakwater at the Water Surface vs. Acceleration for the Breakwater with Vertical Faces and with Inclined Faces, Respectively

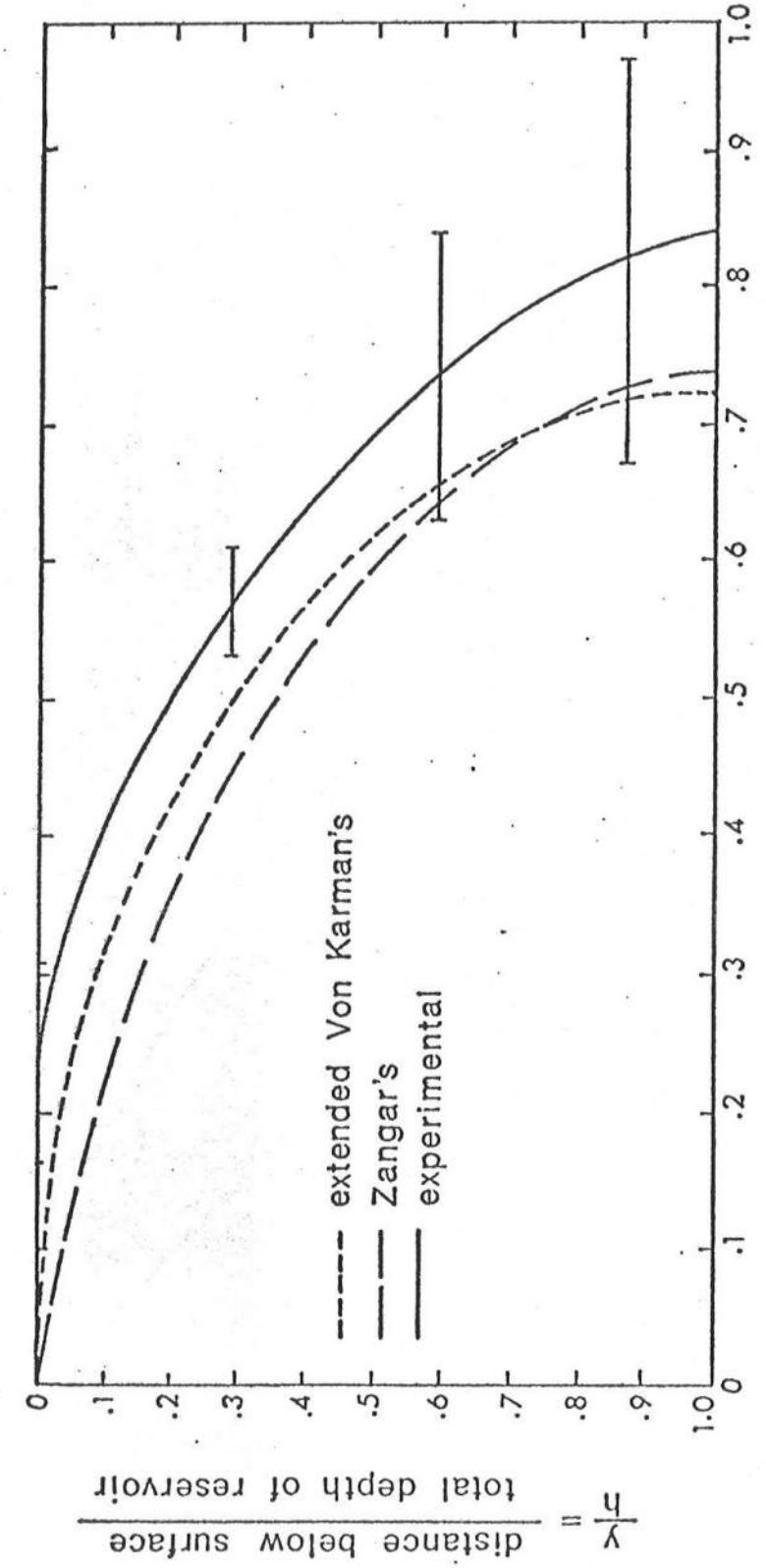

FIGURE 10 Comparison of Pressure Coefficients at Different Elevations on the Breakwater with a Vertical Front Face

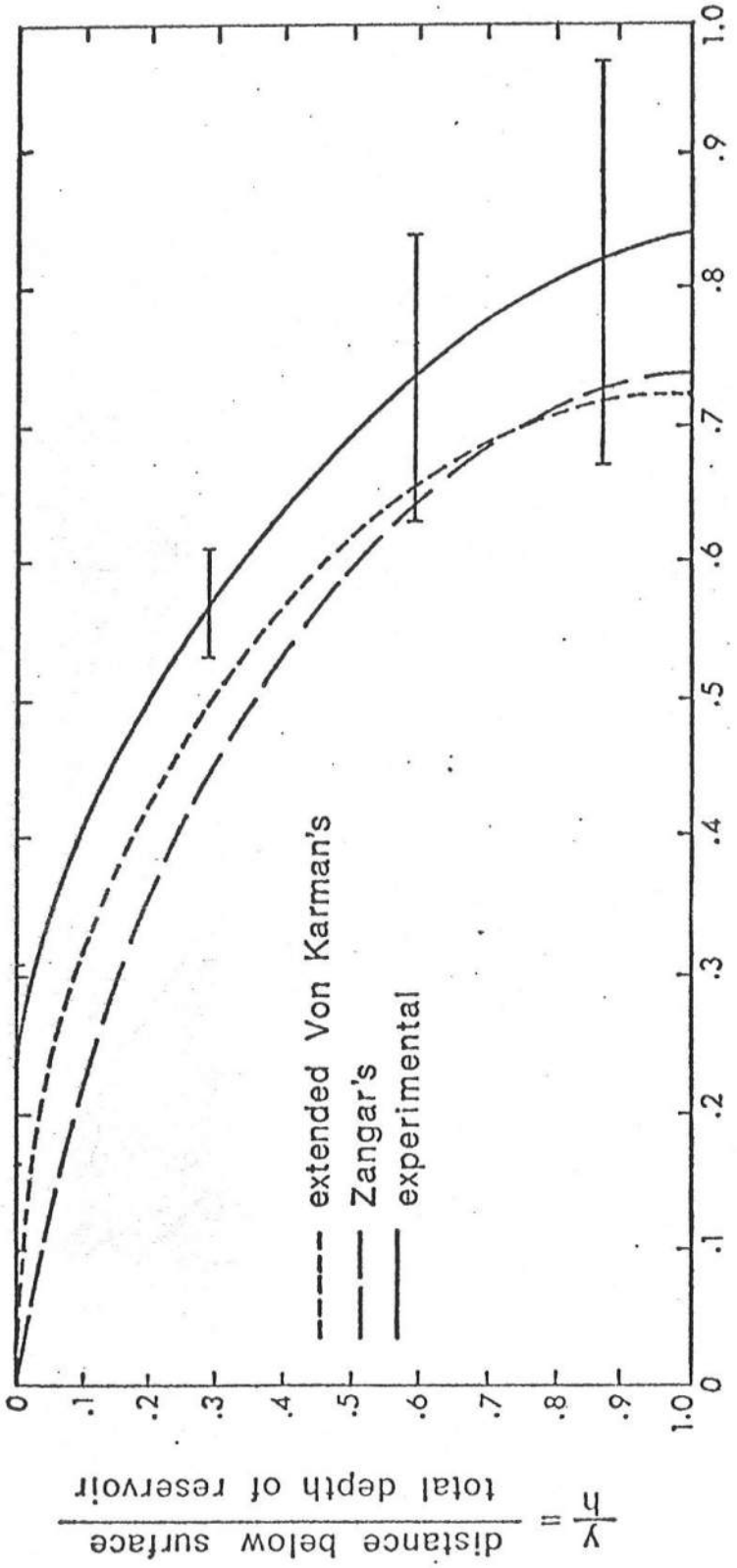

FIGURE 10 Comparison of Pressure Coefficients at Different Elevations on the Breakwater with a Vertical Front Face

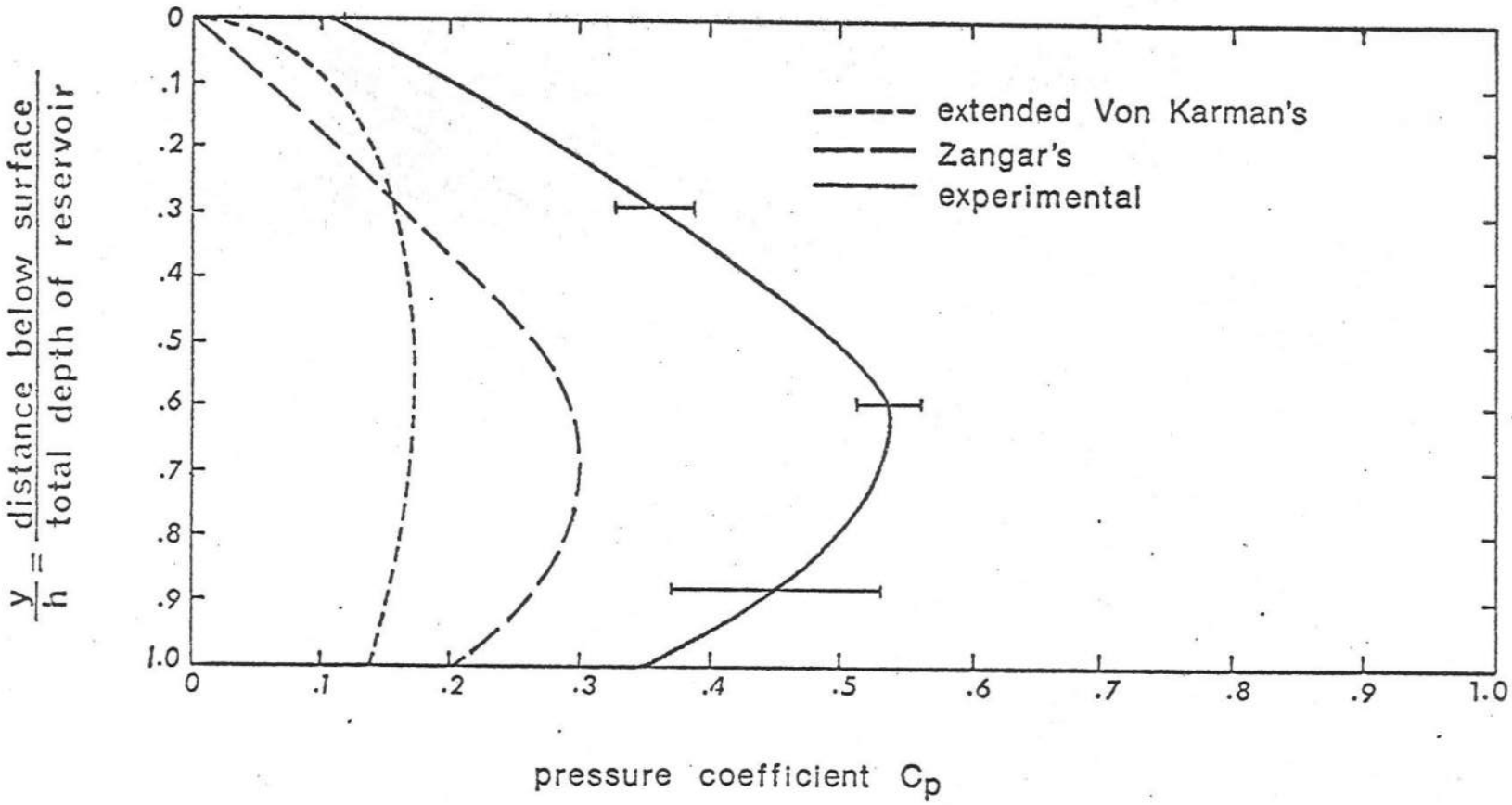

FIGURE 11 Comparison of Pressure Coefficients at Different Elevations on the Breakwater with a 30° Inclined Face

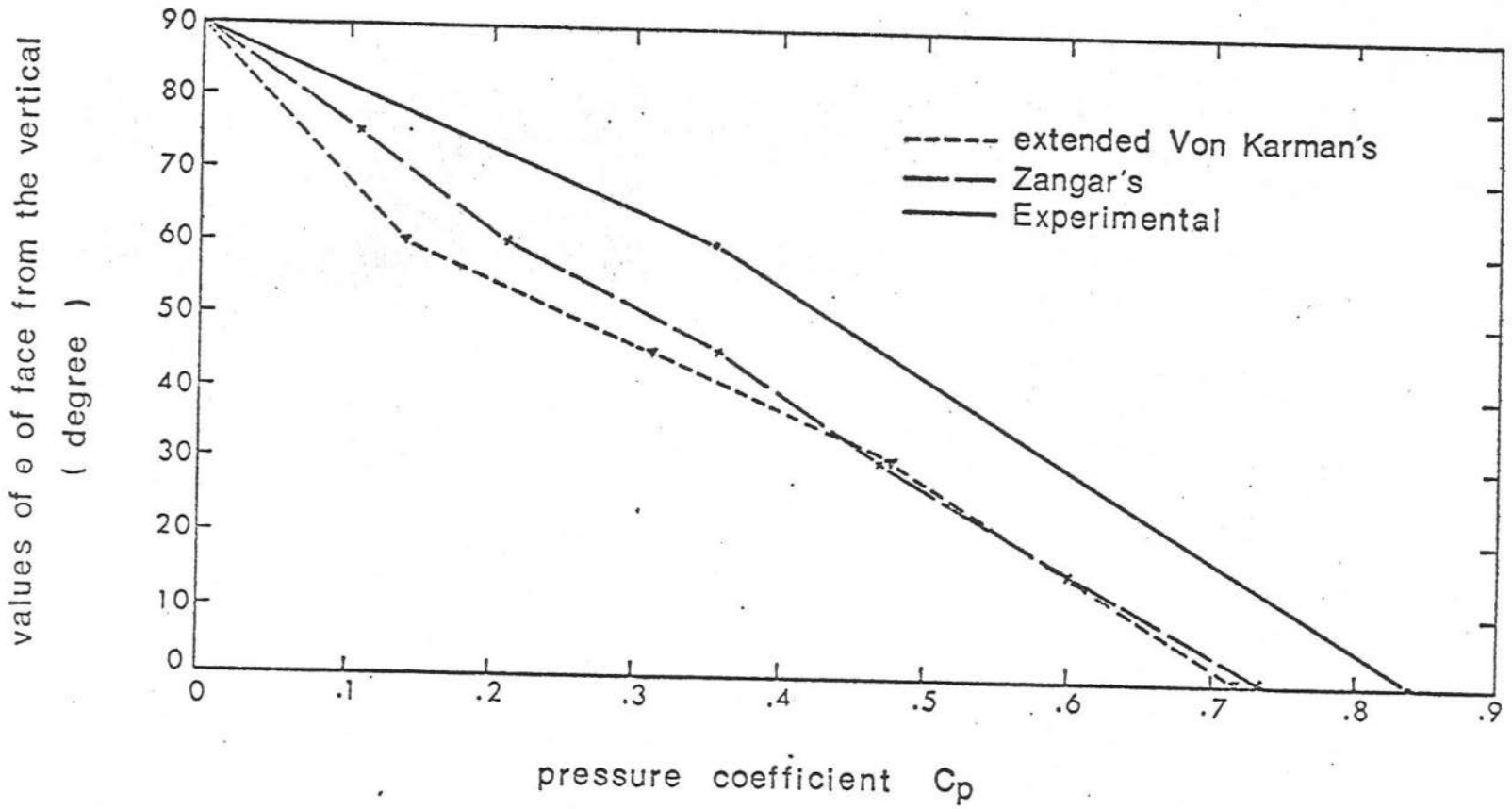

FIGURE 12 Comparison of Pressure Coefficients at the Bottom of the Breakwater for Varied Inclined Angle

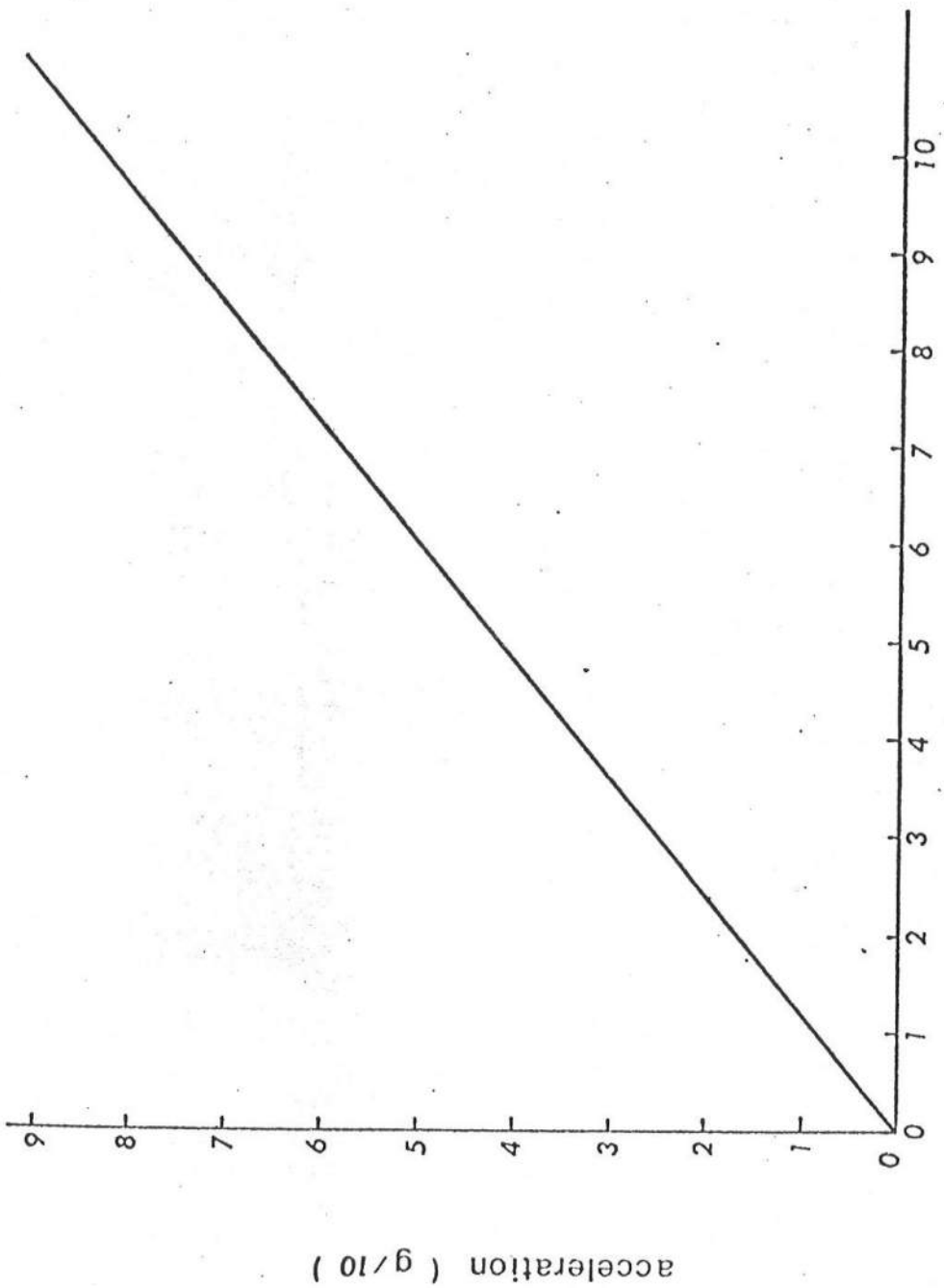

FIGURE 13 Calibration Result of the Statham, Model A5, Accelerometer

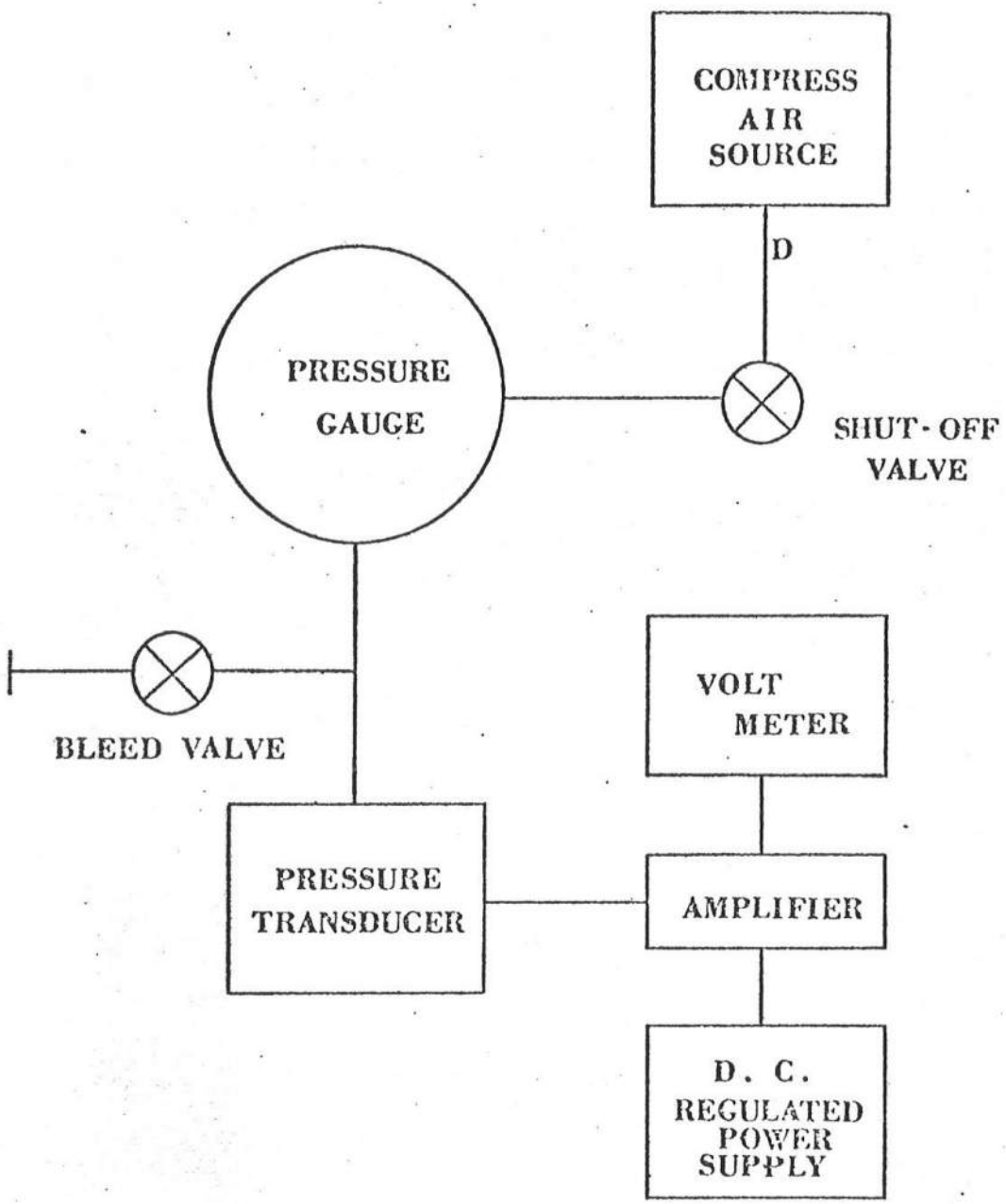

FIGURE 14 A Designed Loop for the Calibration of the Pressure Transducers

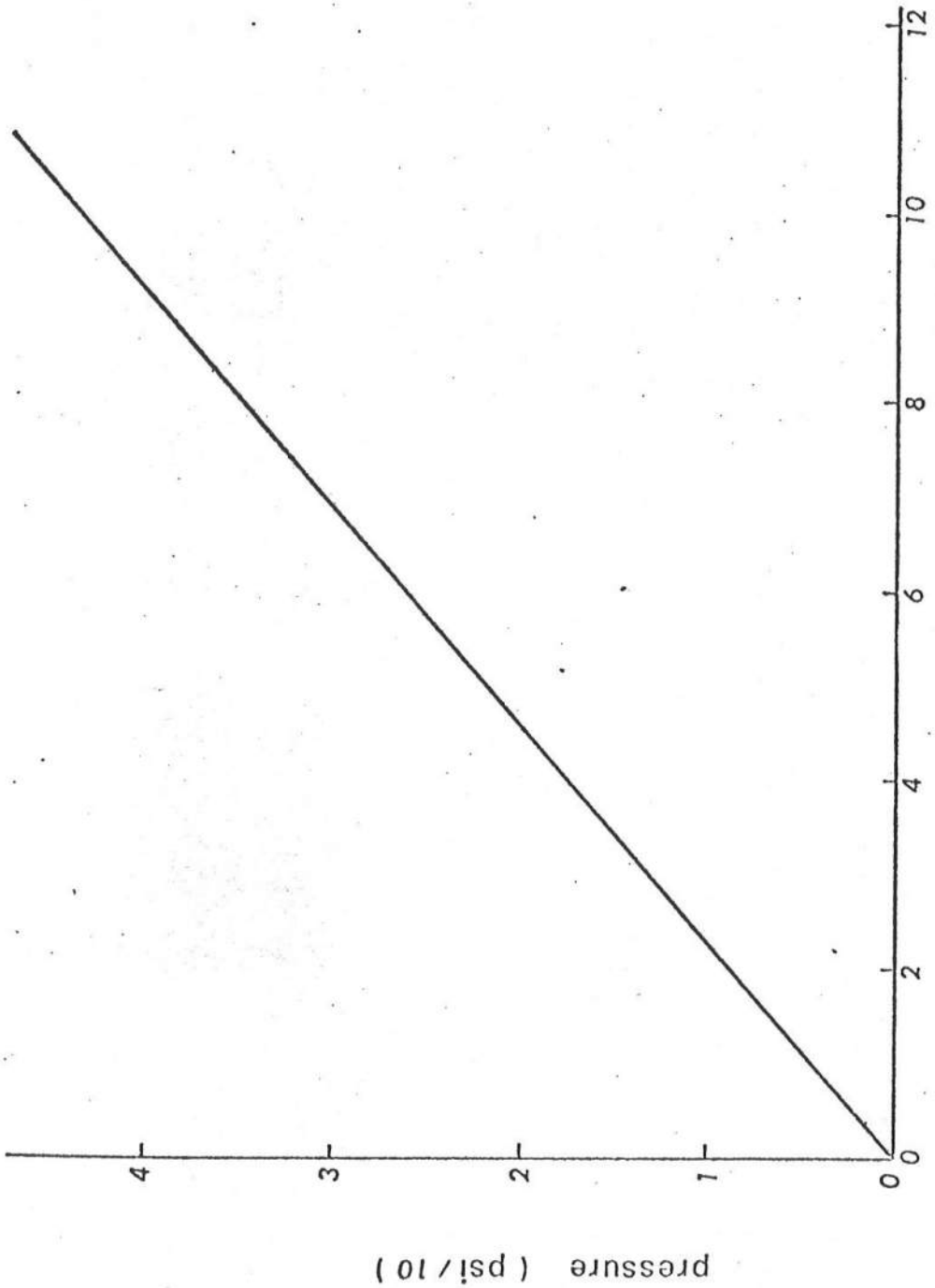

FIGURE 15 Calibration Result of the Viatran, Model 103, Pressure Transducer

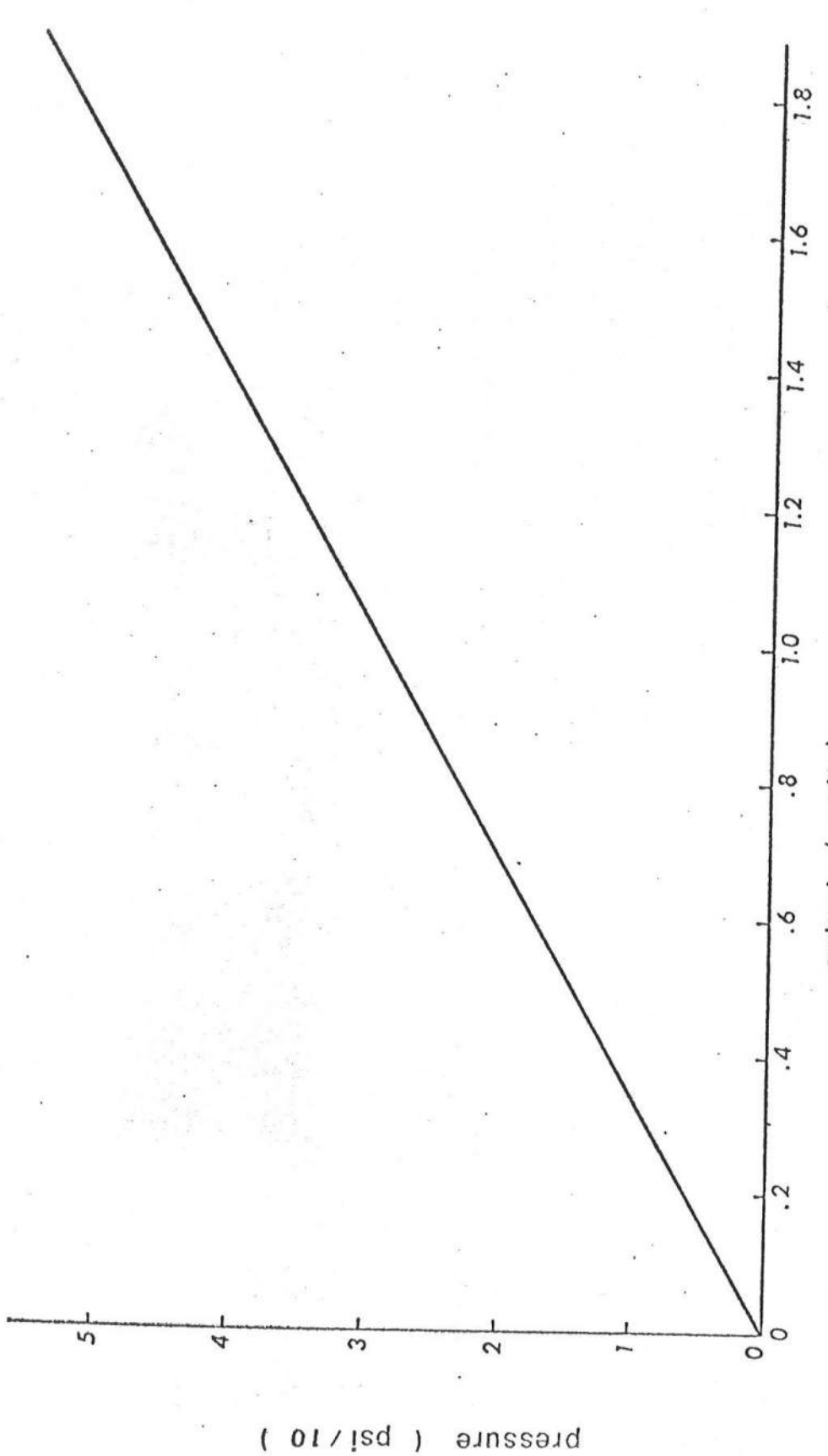

FIGURE 16 Calibration Result of the Statham, Model P131, Pressure Transducer

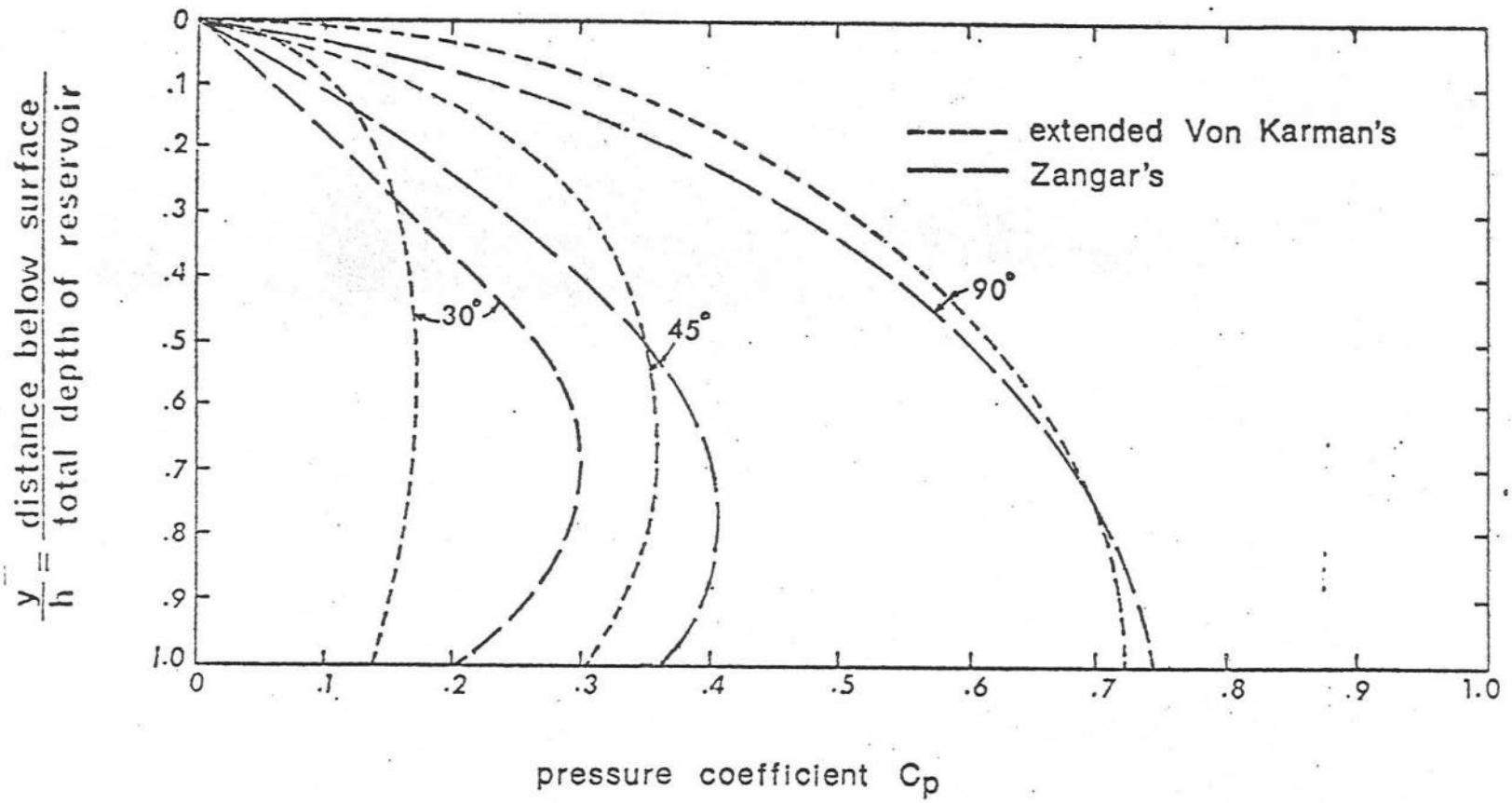

FIGURE 17 Comparison of Pressure Coefficients from Extended Von Kármán's Theory and that from Zangar's Results at Different Elevations.